

Manuscript Number: CATENA4674R1

Title: A novel fluorescent tracer for real-time tracing of clay transport over soil surfaces

Article Type: Research Paper

Keywords: Clay; tracing; soil erosion; diffuse pollution; fluorescence; tracer

Corresponding Author: Prof. John N. Quinton, Ph.D

Corresponding Author's Institution: Lancaster University

First Author: Robert A Hardy, MChem

Order of Authors: Robert A Hardy, MChem; Jacqueline M Pates, PhD; John N. Quinton, Ph.D; Michael P Coogan, PhD

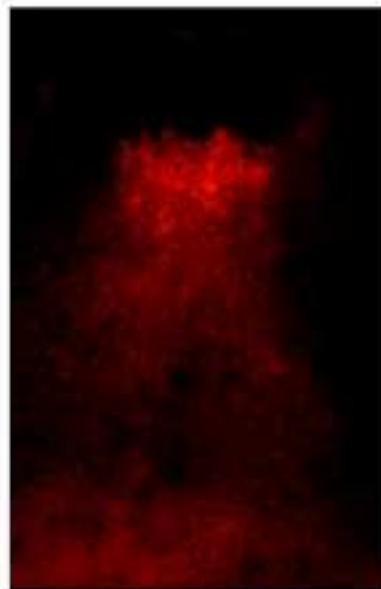
Abstract: Clay is an important vector for the transport of pollutants in the environment, including nutrients, pesticides and metals; therefore, the fate of many chemicals in soil systems is closely linked to that of clay. Understanding the mechanisms responsible for clay transport has been hampered by the lack of a suitable tracer. Producing a tracer that accurately mimics clay transport is challenging, due to the small size of the particles and their unique physical properties. Here we describe the design and synthesis of a tracer using natural clay particles as a foundation, exploiting the natural ability of clay to sorb molecules to coat the clay with a thin layer of fluorophore. Application of the tracer has been demonstrated through the collection of real-time images of the tracer moving over the surface of a soil box during a rainfall event. These images allow, for the first time, clay to be tracked spatially and temporally without need to remove soil for analysis, thus resulting in minimal experimental artefacts. Custom written software has been used to extract high resolution data describing tracer movement and extent throughout the experiment.



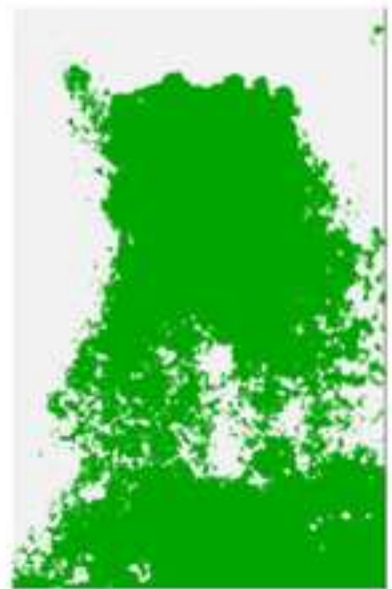
Normal image



Fluorescent image



Fluorescent image



Processed image

Highlights

- A novel clay-sized tracer has been created by labelling Montmorillonite with Rhodamine B.
- The tracer can be detected and tracked in real time and during rainfall events.
- The application of the tracer in soil erosion studies is demonstrated.

1 A novel fluorescent tracer for real-time tracing of
2 clay transport over soil surfaces

3

4 *Robert A. Hardy¹, Jacqueline M. Pates¹, John N. Quinton^{1*}, Michael P. Coogan²*

5

6 ¹Lancaster Environment Center, Lancaster University, Bailrigg, LA1 4YQ

7 ²Chemistry Department, Lancaster University, Bailrigg, LA1 4YQ

8

9 * Corresponding author: j.quinton@lancaster.ac.uk

10

11 **KEYWORDS** Clay; tracing; soil erosion; diffuse pollution; fluorescence; tracer.

12

13

14 **ABSTRACT**

15 Clay is an important vector for the transport of pollutants in the environment, including
16 nutrients, pesticides and metals; therefore, the fate of many chemicals in soil systems is closely
17 linked to that of clay. Understanding the mechanisms responsible for clay transport has been
18 hampered by the lack of a suitable tracer. Producing a tracer that accurately mimics clay
19 transport is challenging, due to the small size of the particles and their unique physical
20 properties. Here we describe the design and synthesis of a tracer using natural clay particles as a
21 foundation, exploiting the natural ability of clay to sorb molecules to coat the clay with a thin
22 layer of fluorophore. Application of the tracer has been demonstrated through the collection of
23 real-time images of the tracer moving over the surface of a soil box during a rainfall event. These
24 images allow, for the first time, clay to be tracked spatially and temporally without need to
25 remove soil for analysis, thus resulting in minimal experimental artefacts. Custom written
26 software has been used to extract high resolution data describing tracer movement and extent
27 throughout the experiment.

28

29

30 **1. Introduction**

31 Clay is a key component of many of the world's soils. Its ability to sorb nutrients, such as
32 phosphorus (Sharpley et al., 1984; Sumner, 2000; Syers et al., 1971), potassium (Petrofanov,
33 2012), metals (Quinton and Catt, 2007) and organic pollutants (Homenauth and McBride, 1994;
34 Sumner, 2000), and its ease of transport in flowing water makes clay an important vector for
35 contaminant transport. Clay particles are moved by both overland flow (Quinton and Catt, 2007;
36 Quinton et al., 2001) and by subsurface flow (McCarthy and Zachara, 1989), which may connect
37 with rivers and lakes. Although studies have developed an empirical understanding of clay
38 movement (Quinton and Catt, 2007; Quinton et al., 2001) and there have been attempts to model
39 clay transport over and through soils (Jarvis et al., 1999; Jomaa et al., 2010), deriving spatial and
40 temporal distributions of clay movement in response to rainfall has proved elusive. In this paper
41 we describe a methodology, which, for the first time, allows the tracking of clay in time and
42 space across a soil surface.

43

44 *1.1 Tracing clay movement*

45 Tracing clay movement has proved very challenging (Armstrong et al., 2012). One aspect of this
46 challenge is the small size of the particles being traced. For larger particles (grains of sand size)
47 there has been success in mixing a dye with a binding agent and then applying this mixture to the
48 surface of the particles (Black et al., 2007). However, this technique has limitations for particles
49 that have a diameter of a few microns, as the coating significantly alters the size and density of
50 the particles. Therefore, for clay an alternative method of tracing is required.

51

52 This has led researchers to develop a range of techniques for tracing clay, including the use of
53 fluorescent microspheres (Burkhardt et al., 2008; Nielsen et al., 2011), rare earth oxides (REOs),
54 which, strictly speaking, are fine silt particles (Stevens and Quinton, 2008; Zhang et al., 2001),
55 and the labelling of clay particles with organic molecules (Selvam et al., 2008). The majority of
56 methods require sampling (via physical removal of material) of the soil after the experiment to
57 determine the tracer concentration (Mabit et al., 2013; Parsons and Foster, 2011). However, it is
58 desirable to understand how a process changes over time requiring the collection of dynamic
59 data. Sampling interferes with detachment and transport processes, limiting the use of existing
60 techniques for process studies. Therefore a method that does not require removal of material is
61 required if progress is to be made in understanding the dynamics of these processes. Additionally
62 there are significant density differences between tracers (such as microspheres and REOs) and
63 native clay particles, which are likely to affect their transport. Therefore a clay tracer with the
64 same physical and chemical properties as the native soil clay, and that can be manufactured
65 easily and analyzed using a non-invasive, non-destructive and in-situ analysis technique
66 operating at moderate to high temporal resolution, is desirable. Some progress has been made in
67 the nano-particle community with the creation of florescent nano-clays, however, no
68 environmental application of the material has been reported (Diaz et al., 2013).

69

70 *1.2 Fluorescence*

71 Fluorescence detection often allows for a high signal to noise ratio permitting single molecule
72 detection (Lakowicz, 2006). This sensitivity enables minimal fluorophore to be used in tracer
73 production, resulting in negligible modification of the coated particle. Traditionally, fluorescence
74 is measured on discrete samples using a fluorimeter, providing detailed spectral information.

75 Two previous studies have captured images of fluorescent tracers using film cameras. In the first,
76 silt-sized glass particles (44 to 2000 μm) labelled with uranium salts, which fluoresce under UV
77 light, were monitored on a 10 m slope inclined at 5.5% (Young and Holt, 1968). Later,
78 fluorescently-labelled pesticide granules (size unknown) were detected in soil, with each
79 photograph imaging 0.63 m^2 (Woods et al., 1999). This work assessed how soil tillage methods
80 affect incorporation of pesticide granules into soil; no effort was made to acquire images of the
81 pesticide moving.

82

83 *1.3 Fluorophore selection*

84 Four principle criteria were used to select the fluorophore. It should: bind strongly to clay;
85 fluoresce at a wavelength different to the auto-fluorescence of soil; be well characterized; and be
86 detectable using a CMOS (Complementary Metal Oxide Sensor) detector in a digital camera.
87 Successful binding relies on matching the fluorophore to the clay of interest; in general the
88 fluorophore should carry the opposite charge to the clay and be lipophilic. Soil auto-
89 fluorescence, due, in part, to the large quantity of organic aromatic acids that are present
90 (excitation maximum at 465 nm, emission maximum at 517 nm) (Milori et al., 2002; Rinnan and
91 Rinnan, 2007), can result in high background fluorescence and therefore interfere with detection
92 of the tracer. Therefore to reduce the impact of natural fluorescence a fluorophore that excites
93 between 520 and 600 nm was desired. Having a well characterized fluorophore allows more
94 rapid progress to be made as its chemical properties are already well described. Finally, we
95 wanted to use a CMOS detector array, commonly found in consumer grade cameras, as they
96 acquire images within the visible range (400-700 nm). A fluorophore that fluoresces in this range
97 was therefore required.

98

99 Rhodamine B was selected as the fluorophore, because: it binds to clay, e.g. Rhodamine B has
100 been shown to bond organically-modified montmorillonite (Diaz et al., 2013), and sodium
101 montmorillonite has been shown to be a successful remediation method for water contaminated
102 with Rhodamine B (Selvam et al., 2008); it typically has an excitation maximum around 570 nm
103 and emission maxima of around 590 nm (Beija et al., 2009), avoiding the most intense soil auto-
104 florescence; and it fluoresces within the range detectable by a CMOS detector. Many derivatives
105 have been synthesized, which could allow fine tuning of the clay tracer's fluorescent properties
106 (Beija et al., 2009), and it is commercially available and inexpensive.

107

108 **2. Materials and Methods**

109 Here we describe the materials and methods used to produces the clay-sized fluorescent tracer,
110 tests of its stability and its application to a laboratory scale erosion experiment.

111

112 The instruments used were an Agilent Technologies Cary Eclipse fluorescence spectrometer and
113 an Agilent Technologies Cary 60 UV/vis absorbance spectrophotometer. Disposable plastic
114 cuvettes were used throughout (Fisher Scientific). The water used was deionized water, unless
115 otherwise specified, and Rhodamine refers to Rhodamine B from Acros Organics (132311000).

116

117 *2.1 Tracer production*

118 The tracer was produced by sorbing Rhodamine onto the surface of clay particles. Twelve grams
119 montmorillonite (69904 ALDRICH) was ground to a fine powder, and sonicated for 30 minutes
120 in water. Rhodamine (0.2 g) was added and the volume made up to 1 L. The mixture was

121 sonicated for a further 45 minutes, stirred for 2 hours, then allowed to settle. The supernatant was
122 clear and colourless, and a vivid red-purple powder was visible at the bottom of the beaker.
123 Excess supernatant was decanted off and the powder collected using vacuum filtration through
124 two Whatman #5 filters. The filtrate was clear and colourless to the eye. The tracer was then
125 thoroughly rinsed using a 50:50 mixture of saturated NaCl and ethanol and then repeatedly with
126 water. The resulting tracer was dried at room temperature in a desiccator and protected from
127 light. If required, the tracer was gently disaggregated by hand before use.

128

129 *2.2 Tracer stability*

130 Stability tests were carried out to ensure the tracer would not degrade over the duration of the
131 trial (less than 24 hours). One gram of tracer (equivalent to 16.7 mg Rhodamine) was placed into
132 100 mL of solvent (either High Ionic Activity Solution (HIAS) or distilled water), and stirred to
133 mix. The HIAS was prepared by combining 25 g NaCl, 4.1 g Na₂SO₄, 0.7 g KCl, 11.2 g
134 MgCl₂·6H₂O and 2.3 g CaCl₂·6H₂O with deionised water to give a final volume of 1 L
135 (Sverdrup et al., 1942). The aim was to produce a simulated natural water of high ionic activity
136 with respect to the major elements. The concentrations used in this solution are extreme
137 compared to those normally found in terrestrial waters; if the tracer is stable under these
138 conditions, we assume that it will be stable in the vast majority of soil environments.

139

140 After a period of time (> 40 h), during which the tracer was allowed to settle, 3 mL of the
141 supernate was placed in a plastic cuvette to assess desorption of Rhodamine from the tracer,
142 using UV/vis absorbance spectrophotometry and fluorescence spectrometry. No attempt to

143 separate the tracer from the water was made, as any particles remaining in suspension were too
144 fine to remove by filtration.

145

146 To make calibration standards, first a stock solution was prepared by dissolving 18.2 mg
147 Rhodamine in 100 mL deionised water. Standards for UV/vis spectrophotometry and
148 fluorescence spectrometry were prepared by diluting the stock 1:250 for fluorescence
149 measurements and 1:125 for UV/vis measurements, using either HIAS or deionised water. Thus,
150 the UV/vis standards contained 0.144 mg Rhodamine per 100 mL, and the fluorescence
151 standards contained 0.072 mg Rhodamine per 100 mL. These are the concentrations that would
152 be achieved had 1% or 0.5% Rhodamine dissolved off the tracer during the stability experiments.

153

154 *2.3 Physical properties of tracer*

155 A Leica confocal microscope was used to record images of clay and tracer particles. Images
156 were taken using a 63x optical lens under oil. The size range of particles was measured using a
157 Malvern Mastersizer 2000.

158

159 *2.4 Acquiring fluorescent images*

160 Images were acquired using a Canon 500-D DSLR camera mounted on a tripod. (See
161 Supplementary Information (SI) 1: Camera setup, for further details of the camera settings and
162 filters). A ~75 mW, 532 nm (green) laser was used to illuminate the soil box, after passing
163 through a rotating diffuser (SI 2: Laser lighting setup, SI: Figure S1). Achieving uniform
164 illumination is critical to producing accurate images (Waters, 2009). Visual and photographic
165 assessment of the light showed an acceptable degree of uniformity (SI: Figure S2).

166

167 2.5 Soil box

168 Perspex soil boxes (350 mm by 500 mm), with drainage holes in the base, were filled with 4 cm
169 fine gravel, landscape fabric membrane, 3 cm sand and 4 cm soil (screened to 4 mm) to simulate
170 natural infiltration conditions following Armstrong *et al.*'s method (Armstrong et al., 2012). A
171 150 x 50 x 5 mm section of soil was removed, mixed with 4 g of tracer and then replaced (Figure
172 1). To bring them to near saturation, the soil boxes were immersed in water, to a depth 1 cm
173 above the soil-sand interface, for 22 hours. The box was then drained for one hour and exposed
174 to rainfall, while set at a slope of 4%.

175

176 2.6 Rainfall

177 A gravity-fed rainfall simulator was used to deliver rainfall with an intensity of 42 mm h⁻¹ using
178 reverse osmosis (RO) grade water (Armstrong et al., 2012).

179

180 2.7 Runoff testing

181 Runoff was collected from the run-off collector (Figure 1), with the container receiving the run-
182 off changed every 5 minutes. Runoff collected from between 30 and 45 minutes after rainfall has
183 commenced was bulked and vacuum filtered using two Whatman #5 filters to remove the
184 particulates.

185

186

187 **3. Results**

188 *3.1 Tracer stability*

189 In order for a tracer to be useful it must remain intact for the duration of the study. The most
190 likely route of tracer degradation is desorption of Rhodamine from the clay surface. To
191 investigate this possibility, UV/vis absorbance and fluorescence spectrometry were used to
192 characterize the loss of Rhodamine upon exposure to HIAS or distilled water (over 40 hours).

193

194 The supernate showed virtually no absorbance of light in the UV/vis range due to solution phase
195 Rhodamine, as demonstrated by the lack of a peak at ~ 560 nm (Figures 2a and b). Figure 2a
196 shows a raised baseline attributed to fine, colloidal-sized particulate matter (the tracer) remaining
197 in suspension scattering the light, a hypothesis supported by the lack of specific absorption
198 bands. The small peak at ~ 590 nm is assigned to Rhodamine as no other component absorbs in
199 that region. However the wavelength maximum does not match that of the Rhodamine standard,
200 which suggests that the Rhodamine responsible for this peak is modified compared to the
201 standard. An interaction between Rhodamine and montmorillonite, either through chemisorption
202 onto the surface, or simple protonation (the montmorillonite used is pH 3), could account for this
203 shifted wavelength. The absence of a raised baseline in HIAS (Figure 2b) suggests that there are
204 no tracer particles present; we propose that the high ionic strength of HIAS encourages
205 flocculation and hence precipitation out of the clay tracer (Elimelech et al., 1995).

206

207 Fluorescence measurements showed a peak with a maximum emission at 575 nm, attributed to
208 dissolved Rhodamine, in the HIAS solution (Figure 2d). In order to estimate the amount of
209 Rhodamine lost from the tracer during the experiment, linearity between the sample and standard

210 was assumed and the following equation used to estimate the amount of Rhodamine lost:
211 $(\text{standard concentration} / \text{fluorescence intensity of standard}) \times \text{fluorescence intensity of sample}$.
212 This relationship suggests that approximately 0.022 mg Rhodamine was lost from the tracer, i.e.
213 0.13% of the total amount used in the experiment. A broader and flatter peak is seen in the
214 deionized water sample (Figure 2c), indicative of minimal desorption from the tracer. The
215 greater desorption of Rhodamine in HIAS is probably due to the high ionic strength of the
216 solution, whereby the HIAS ions compete with the Rhodamine for binding sites on the clay
217 forcing the latter to desorb. However, HIAS has a much higher ionic strength than water soil
218 mixtures, where the tracer will be deployed; therefore it is reasonable to assume that desorption
219 will not readily occur during soil transport experiments.

220

221 *3.2 Physical properties of tracer*

222 Comparing the particle size distribution of the tracer and the clay from which the tracer was
223 made, it was found that 55% of the tracer had a size of less than 2 μm , compared to 51% of the
224 montmorillonite. Furthermore, the size distribution of the particles before and after treatment
225 with Rhodamine was consistent (SI 3: Tracer size). Confocal microscope images show that the
226 particles retain their irregular sizes and shapes (Figures 3a and b). The Rhodamine appears to be
227 uniformly distributed over the particle surface, without disturbing surface texture (Figure 3c).
228 The appearance of more rings around the clay in the phase contrast image of the tracer is
229 consistent with the hydration of the clay during synthesis of the tracer.

230

231 *3.3 Tracer movement images*

232 The images show, for the first time, clay movement over a soil surface in real time under
233 continuous simulated rainfall conditions (Figure 4 and SI 4: Images). The movement of tracer
234 across the whole soil box was recorded every 7 s from a distance of ~ 2 m. The sample area is
235 2431 x 1769 pixels (0.135 m²), which equates to approximately 31 pixels per mm². As no soil
236 was physically removed from the box during the experiment, there was no external disturbance
237 to the system, resulting in fewer sampling artefacts. By increasing the light input (by increasing
238 the camera aperture and moving the light source closer to the target) and sensitivity of the CMOS
239 detector (by increasing the ISO setting), the soil box was imaged on the sub-second time scale
240 (every 0.8 s), although increased noise was present (SI 5: Rapid imaging).

241

242 *3.4 Image processing*

243 Although it is possible to view the images without post-processing, much can be gained from
244 doing so. Using [R] (Hijmans, 2014; Polzehl and Tabelow, 2007; R Development Core Team,
245 2013; Urbanek, 2013), the images were converted to false colour with noise suppressed (Figure
246 4). Further details of the image processing methods can be found in SI 6: Image processing.
247 These images were easier to analyze visually, as they show presence of tracer in green and the
248 absence in white. The file size of the images is approximately 100 times smaller than the original
249 images. Images of this nature were then compressed (Cinepak codec by Radius, quality 100) into
250 a time-lapse video using VirtualDub (version 1.10.4) allowing the whole event to be reviewed in
251 less than a minute.

252

253 The intensity of fluorescence from the tracer, in the solid state, is independent of the
254 concentration of tracer. This type of behavior is symptomatic of self-quenching, which involves
255 the rapid exchange of energy between molecules and de-excitation via non-radiative processes,
256 typically relaxation to the ground state through vibrational levels. Due to the close spatial
257 proximity of the Rhodamine molecules to one another when bound to clay and the small Stokes
258 shift (and therefore overlap of excitation and emission bands), this type of behavior is neither
259 unusual nor unexpected (Lakowicz, 2006). As the amount of light emitted from the tracer is not a
260 function of the tracer concentration, the intensity of light cannot be used to quantify the amount
261 of tracer at a given point. Nonetheless, the true-colour images shown (Figures 4a-c) have some
262 qualitative properties, as areas that are much more intensely coloured are likely to contain more
263 tracer than those that are less intensely coloured.

264

265 We have confidence that interference due to autofluorescence was not a problem as we have
266 used constant illumination and the initial images (Figures 4a and 4d) show intense colour where
267 the tracer was applied and virtually no colour anywhere else.

268

269 *3.5 Runoff testing*

270 In order for the tracer to be useful it must remain intact throughout the experiment, which can be
271 evaluated by recovering the tracer afterwards. Particulate material recovered from the runoff,
272 was dried and photographed on a black (non-fluorescent) background (Figure S4). The colour
273 and intensity seen in Figure S4 are very similar to the colour and intensity seen in Figure 4,
274 suggesting that the tracer has remained intact throughout the experiment.

275

276 The filtrate was a reddish brown to the eye, which were attributed to fine particles, given that
277 they are illuminated when a ~ 1 mW (532 nm) laser beam is passed through the suspension (an
278 effect not seen in particle-free solutions). The filtrate was centrifuged at 15000 rpm for 99
279 minutes, the supernatant decanted and then imaged on a non-fluorescent background, using
280 standard image acquisition and processing parameters. No fluorescence was seen (Figure 5), in
281 contrast to a solution containing 2 µg/L Rhodamine, which could be readily detected. We are
282 therefore confident that the images in Figures 4 a, b, c are images of the Rhodamine-labeled clay
283 rather than Rhodamine in solution.

284

285 *3.6 Demonstration of application*

286 In order to demonstrate how high temporal and spatial resolution data can be used in the study of
287 soil erosion processes, the tracer front was mapped against time (Figure 6a). The data were
288 extracted from 312 images using a custom written function in [R] (SI 10: Tracking tracer
289 spread). The effect of rain-splash was analyzed by looking at how the tracer front moved up and
290 down the box (Figure 6a), which demonstrates the dynamic nature of both the upper and lower
291 tracer fronts. As expected the movement down the box is more rapid than that up the box. The
292 lower tracer front moves rapidly to begin with, slows and then moves rapidly again. We attribute
293 this behavior to changes in soil microtopography akin to a dam bursting, allowing overland flow
294 to connect with the bottom of the box and rapidly deliver the tracer. The spike at approximately
295 1000 s is attributed to an artefact in the data. Lateral spreading of the tracer was also noticed in
296 the images so a plot correlating the width of the tracer band to time was also produced (Figure
297 6b), as well as the changing tracer area over time (Figure 6c). The development of the tracer
298 area can viewed dynamically in the online version of the papers (video1).

299

300 **4. Discussion**

301 We have developed a tracing and imaging method that, for the first time, allows clay movement
302 to be traced, with mm precision in two dimensions with a time-step of approximately 1 s, under
303 simulated rainfall conditions without the need to stop the experiment to take samples. This is a
304 major advance over previously reported techniques. Previous work has focused on the use of
305 exotic particles and elemental tagging in soil tracing; examples include fluorescent microspheres
306 (Pryce, 2011), ceramic prills (Duke et al., 2000; Plante et al., 1999), plastic magnetic beads
307 (Ventura et al., 2001) and REOs (Deasy and Quinton, 2010). These methods have been criticized
308 as the tracers have different physical properties, such as size, shape and density, to the target soil
309 (Zhang et al., 2003). By using natural particles as the basis for this tracer we believe that we have
310 minimised or avoided many of these problems; physically, the tracer retains the same size and
311 density characteristics as the native clay and aggregates in the same way as the untreated clay.

312

313 The second advantage over existing methods is to ability to capture spatial information, without
314 the need to destructively sample the experiment, and temporal information throughout the
315 experiment, allowing highly dynamic changes in tracer distribution to be captured. With the
316 exception of Armstrong et al. (Armstrong et al., 2012), who used magnetic susceptibility to non-
317 destructively determine the position of a magnetic tracer at the end of an experiment,
318 experimenters have relied on destructive sampling at the end of an experiment in order to
319 understand surface processes. Destructive sampling has limited spatial resolution, because of the
320 size of samples required (typically $> 2 \text{ cm}^2$), is laborious, and for many tracers requires
321 subsequent analysis. The temporal and spatial resolution of our tracer will allow us to gain

322 insights into the controls on colloidal detachment and transport, and have the potential to enable
323 the spatial testing of distributed models of size-selective erosion processes (Heng et al., 2011).

324

325 The system we have described is limited in scale to a 0.5 m x 0.4 m soil box, constrained by the
326 field of view of the camera as well as the area that can be illuminated with the laser. Larger fields
327 of view could be used to expand the area that can be imaged; however this would reduce the
328 resolution of the system. Working on larger study areas will require a brighter laser for
329 illumination and either multiple cameras to capture multiple images, which could be stitched
330 together in post-processing, or a super-camera with a large frame area and high density of pixels,
331 for example the qG (Aqueti Inc.), which is 250 megapixel camera with a 50 by 24 degree field of
332 view.

333

334 This new tracing methodology will open up new opportunities to understand clay transport and
335 associated pollutants and nutrients, helping us to develop a better understanding of these
336 dynamic processes. There is potential to develop the system further to provide a tracer and
337 detection method for field-based deployment and the quantification of tracer concentrations,
338 opening up new possibilities for understanding the fate and behavior of sediment and
339 contaminants in the environment.

340

341 **Supporting Information.** Diagrams relating to equipment design, camera and lighting
342 conditions, computer code, runoff testing and demonstration of application can be found in the
343 Supporting Information.

344

345 **Acknowledgments**

346 R.H. is funded by a joint U.K. Natural Environment Research Council – Analytical Chemistry
347 Trust Fund studentship (NE/J017795/1). Thanks to Mike James for his support with image
348 processing and Debbie Hurst for microscope images.

349

350 **References**

351 Armstrong, A., Quinton, J.N. and Maher, B.A., 2012. Thermal enhancement of natural
352 magnetism as a tool for tracing eroded soil. *Earth Surf. Proc. Land.* 37, 1567-1572.

353 Beija, M., Afonso, C.A.M. and Martinho, J.M.G., 2009. Synthesis and applications of
354 Rhodamine derivatives as fluorescent probes. *Chemical Soc. Rev.* 38, 2410-2433.

355 Black, K.S., Athey, S., Wilson, P. and Evans, D. (2007) *Coastal and Shelf Sediment Transport*.
356 Balson, P.S. and Collins, M.B. (eds), pp. 73-91, Geological Society, Special Publications,
357 London.

358 Burkhardt, M., Kasteel, R., Vanderborght, J. and Vereecken, H., 2008. Field study on colloid
359 transport using fluorescent microspheres. *Eur. J. Soil Sci.* 59, 82-93.

360 Deasy, C. and Quinton, J.N., 2010. Use of rare earth oxides as tracers to identify sediment source
361 areas for agricultural hillslopes. *Solid Earth* 1, 111-118.

362 Diaz, C.A., Xia, Y., Rubino, M., Auras, R., Jayaraman, K. and Hotchkiss, J., 2013. Fluorescent
363 labeling and tracking of nanoclay. 5, 164-168.

364 Duke, M.J.M., Plante, A.F. and McGill, W.B., 2000. Application of INAA in the characterisation
365 and quantification of Dy-labeled ceramic spheres and their use as inert tracers in soil
366 studies. *J. Radioanal. Nucl. Ch.* 244, 165-171.

367 Elimelech, M., Gregory, J., Jia, X. and Williams, J.A., 1995. Particle Deposition and
368 Aggregation : Measurement, Modelling and Simulation, Butterworth-Heinemann,
369 Oxford, England.

370 Heng, B.C.P., Sander, G.C., Armstrong, A., Quinton, J.N., Chandler, J.H. and Scott, C.F., 2011.
371 Modeling the dynamics of soil erosion and size-selective sediment transport over
372 nonuniform topography in flume-scale experiments. *Water Resources Res.* 47, W02513.

373 Hijmans, R.J. (2014) raster: raster: Geographic data analysis and modeling.

374 Homenauth, O.P. and McBride, M.B., 1994. Adsorption of aniline on layer silicate clays and an
375 organic soil. *Soil Sci. Soc. Am. J.* 58, 347-354.

376 Jarvis, N.J., Villholth, K.G. and Ulen, B., 1999. Modelling particle mobilization and leaching in
377 macroporous soil. *Eur. J. Soil Sci.* 50, 621-632.

378 Jomaa, S., Barry, D.A., Brovelli, A., Sander, G.C., Parlange, J.Y., Heng, B.C.P. and Tromp-van
379 Meerveld, H.J., 2010. Effect of raindrop splash and transversal width on soil erosion:
380 Laboratory flume experiments and analysis with the Hairsine-Rose model. *J. Hydrol.*
381 395, 117-132.

382 Lakowicz, J.R., 2006. Principles of Fluorescence Spectroscopy, Springer, New York.

383 Mabit, L., Meusbürger, K., Fulajtar, E. and Alewell, C., 2013. The usefulness of ¹³⁷Cs as a tracer
384 for soil erosion assessment: A critical reply to Parsons and Foster (2011). *Earth-Sci. Rev.*
385 127, 300-307.

386 McCarthy, J.F. and Zachara, J.M., 1989. Subsurface transport of contaminants. Mobile colloids
387 in the subsurface environment may alter the transport of contaminants. *Environ. Sci.*
388 *Technol.* 23, 496-502.

389 Milori, D., Martin-Neto, L., Bayer, C., Mielniczuk, J. and Bagnato, V.S., 2002. Humification
390 degree of soil humic acids determined by fluorescence spectroscopy. *Soil Sci.* 167, 739-
391 749.

392 Nielsen, M.H., Styczen, M., Ernstsén, V., Petersen, C.T. and Hansen, S., 2011. Distribution of
393 bromide and microspheres along macropores in and between drain trenches. *Vadose Zone*
394 *J.* 10, 345-353.

395 Parsons, A.J. and Foster, I.D.L., 2011. What can we learn about soil erosion from the use of Cs-
396 137? *Earth-Sci. Rev.* 108, 101-113.

397 Petrofanov, V.L., 2012. Role of the soil particle-size fractions in the sorption and desorption of
398 potassium. *Eurasian Soil Sci.* 45, 598-611.

399 Plante, A.F., Duke, M.J.M. and McGill, W.B., 1999. A tracer sphere detectable by neutron
400 activation for soil aggregation and translocation studies. *Soil Sci. Soc. Am. J.* 63, 1284-
401 1290.

402 Polzehl, J. and Tabelow, K., 2007. Adaptive smoothing of digital images: the R package
403 *adimpro*. *J. Statistical Software.*

404 Pryce, O. (2011) Development of environmental tracers for sediments and phosphorus. PhD
405 thesis, Lancaster University.

406 Quinton, J.N. and Catt, J.A., 2007. Enrichment of heavy metals in sediment resulting from soil
407 erosion on agricultural fields. *Environ. Sci. Technol.* 41, 3495-3500.

408 Quinton, J.N., Catt, J.A. and Hess, T.M., 2001. The selective removal of phosphorus from soil: Is
409 event size important? *J. Environ. Qual.* 30, 538-545.

410 R Development Core Team (2013) *R: A Language and Environment for Statistical Computing.*

411 Rinnan, R. and Rinnan, Å., 2007. Application of near infrared reflectance (NIR) and
412 fluorescence spectroscopy to analysis of microbiological and chemical properties of
413 Arctic soil. *Soil Biol. Biochem.* 39, 1664-1673.

414 Selvam, P.P., Preethi, S., Basakaralingam, P., N.Thinakaran, Sivasamy, A. and Sivanesan, S.,
415 2008. Removal of rhodamine B from aqueous solution by adsorption onto sodium
416 montmorillonite. *J. Hazard. Mater.* 155, 39-44.

417 Sharpley, A.N., Smith, S.J., Stewart, B.A. and Mathers, A.C., 1984. Forms of phosphorus in soil
418 receiving cattle feedlot waste. *J. Environ. Qual.* 13, 211-215.

419 Stevens, C.J. and Quinton, J.N., 2008. Investigating source areas of eroded sediments transported
420 in concentrated overland flow using rare earth element tracers. *Catena* 74, 31-36.

421 Sumner, M.E., 2000. *Handbook of Soil Science*, CRC Press, Boca Raton, Fla.

422 Sverdrup, H.U., Johnson, M.W. and Fleming, R.H., 1942. *The Oceans, Their Physics,*
423 *Chemistry, and General Biology*, Prentice-Hall, inc., New York.

424 Syers, J.K., Evans, T.D., Williams, J.D. and Murdock, J.T., 1971. Phosphate sorption parameters
425 of representative soils from Rio Grande Do Sul, Brazil. *Soil Sci.* 112, 267-275.

426 Urbanek, S. (2013) tiff: Read and write TIFF images.

427 Ventura, E., Nearing, M.A. and Norton, L.D., 2001. Developing a magnetic tracer to study soil
428 erosion. *Catena* 43, 277-291.

429 Waters, J.C., 2009. Accuracy and precision in quantitative fluorescence microscopy. *J. Cell Biol.*
430 185, 1135-1148.

431 Woods, S., Haydock, P.P.J., Evans, K., Robinson, R.C. and Dawkins, T.C.K., 1999. Use of
432 fluorescent tracer techniques and photography to assess the efficiency of tillage
433 incorporated granular nematicides into potato seed-beds. *Soil Tillage Res.* 51, 17-23.

434 Young, R.A. and Holt, R.F., 1968. Tracing soil movement with fluorescent glass particles. Soil
435 Sci. Soc. Am. Pro. 32, 600-602.

436 Zhang, X.C., Friedrich, J.M., Nearing, M.A. and Norton, L.D., 2001. Potential use of rare earth
437 oxides as tracers for soil erosion and aggregation studies. Soil Sci. Soc. Am. J. 65, 1508-
438 1515.

439 Zhang, X.C., Nearing, M.A., Polyakov, V.O. and Friedrich, J.M., 2003. Using rare-earth oxide
440 tracers for studying soil erosion dynamics. Soil Sci Soc Am J 67, 279-288.

441

Figure

Figure 1. Schematic of the soil box used showing starting location of tracer. The grey area is the imaged area.

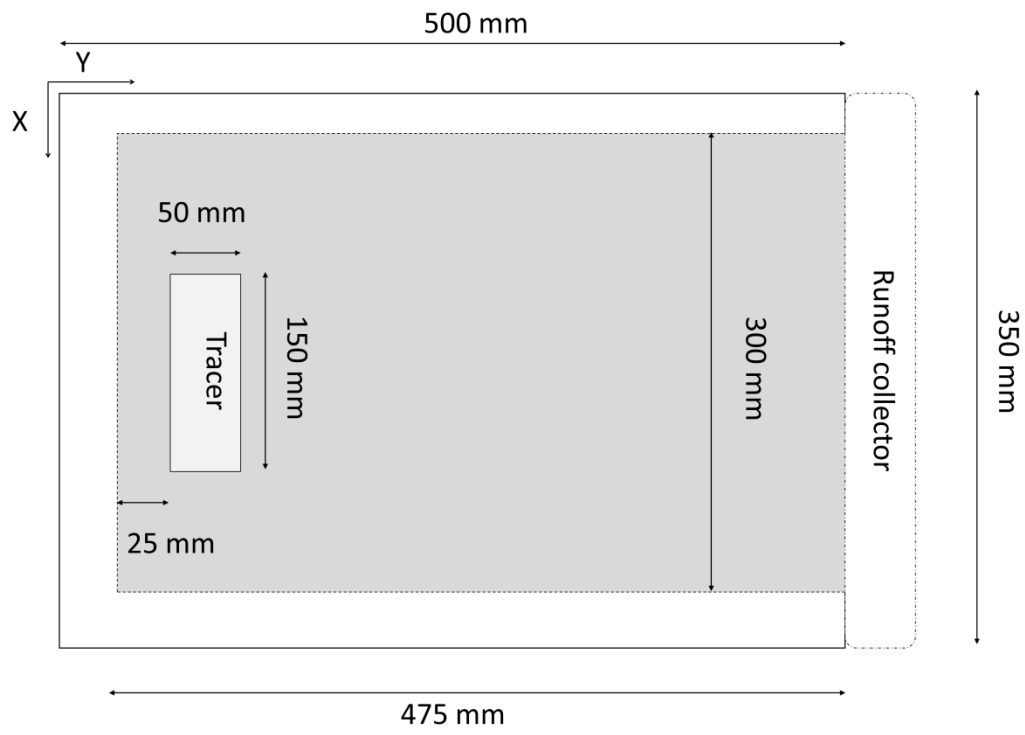


Figure 2. UV/vis (A and B) and fluorescence spectra (C and D) of supernatant solutions. The tracer was mixed with either deionised water (A and C) or high ionic activity solution (B and D) and the supernatant separated after more than 40 hours, to test for desorption of Rhodamine.

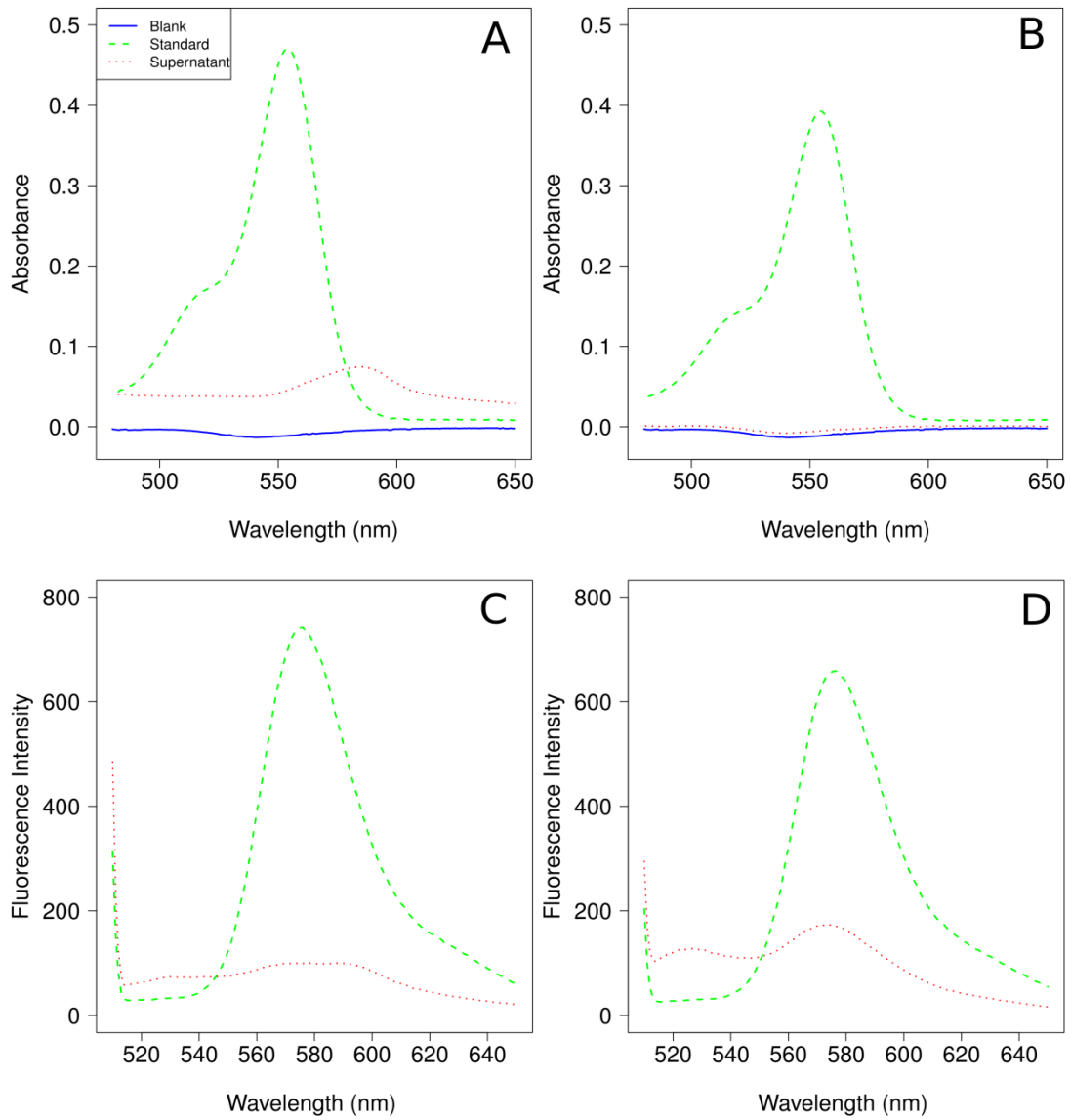


Figure 3. Confocal micrographs of clay tracer: A) phase contrast before treatment with Rhodamine; B) phase contrast after treatment with Rhodamine; and C) false colour fluorescent after treatment with Rhodamine. Note that they clay retains its size and shape after treatment and that the fluorescence appears quite uniformly on the clays surface.

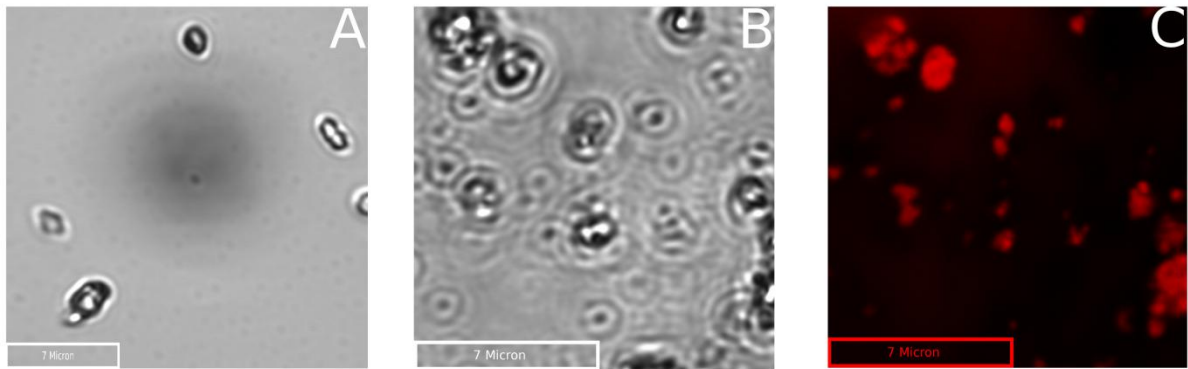


Figure 4. Images of soil box (top of box at top of image) showing tracer location at various times. A to C are true color images and D to F are false color images produced using [R]. A and D were before exposure to rain, B and E are after 262 s of rain and C and F are after 2252 s. After 0 seconds the tracer was constrained to the area where it was applied. After 262 s the tracer had moved down the box and spread laterally, further movement and lateral spreading continued until the experiment was ended at 2252 s. Transport pathways of clay from the top of the box to the bottom can be observed together with a depositional area which formed at the bottom edge of the box.

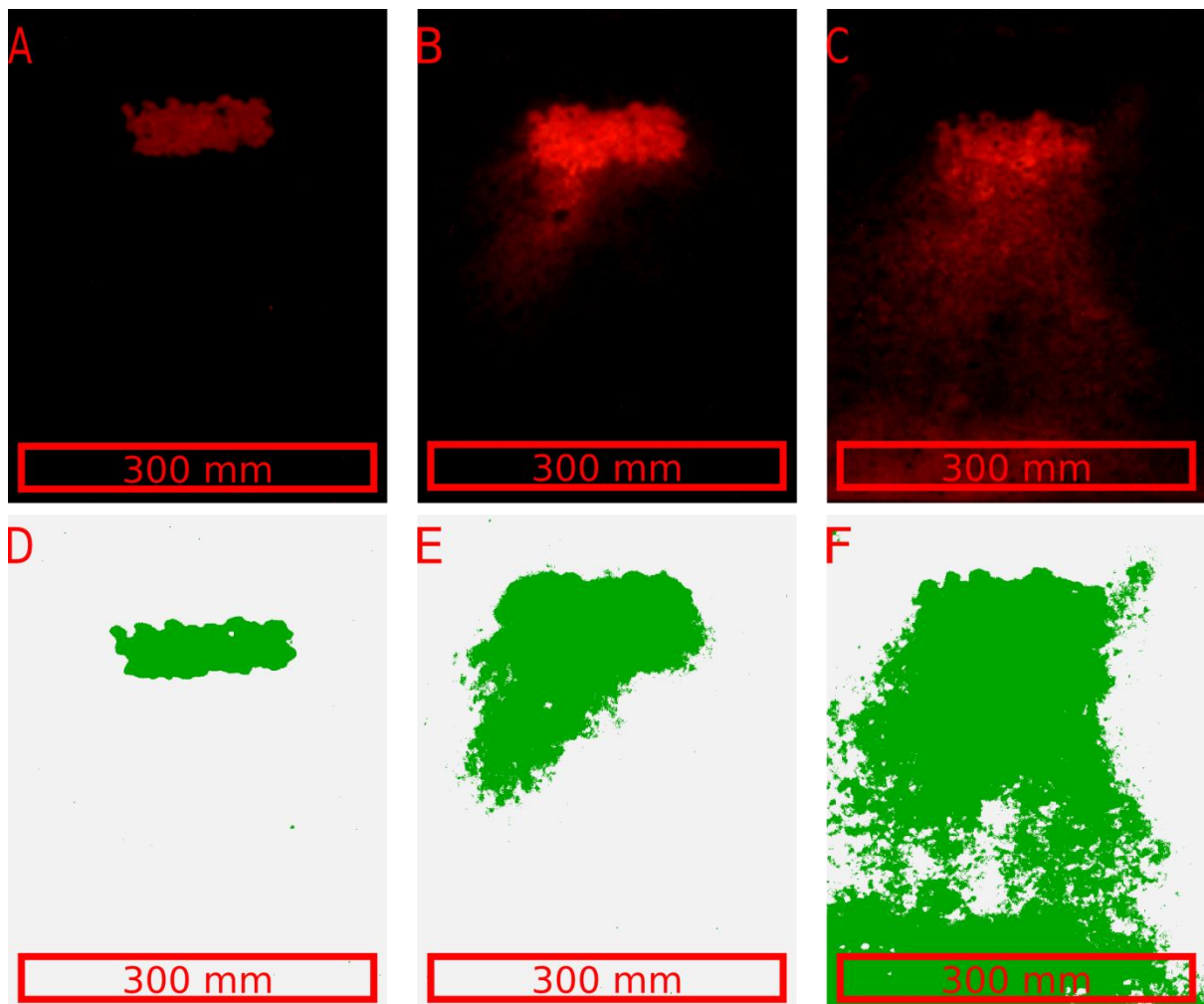


Figure 5: Comparison of soil-box runoff in a petri dish backed with black plastic after filtration and ultra-centrifugation with a Rhodamine standard. The solid circles show the location of the standard (2 $\mu\text{g/L}$) while the dotted circles shows the filtered and ultra-centrifuged soil-box runoff. A is a true colour image captured under typical room lighting with a 570 nm long pass filter on the camera, B is a recorded using 532nm lighting and a 570 nm filter, and C is a false colour image process using R. The standard is clearly detectable in C but not the runoff.

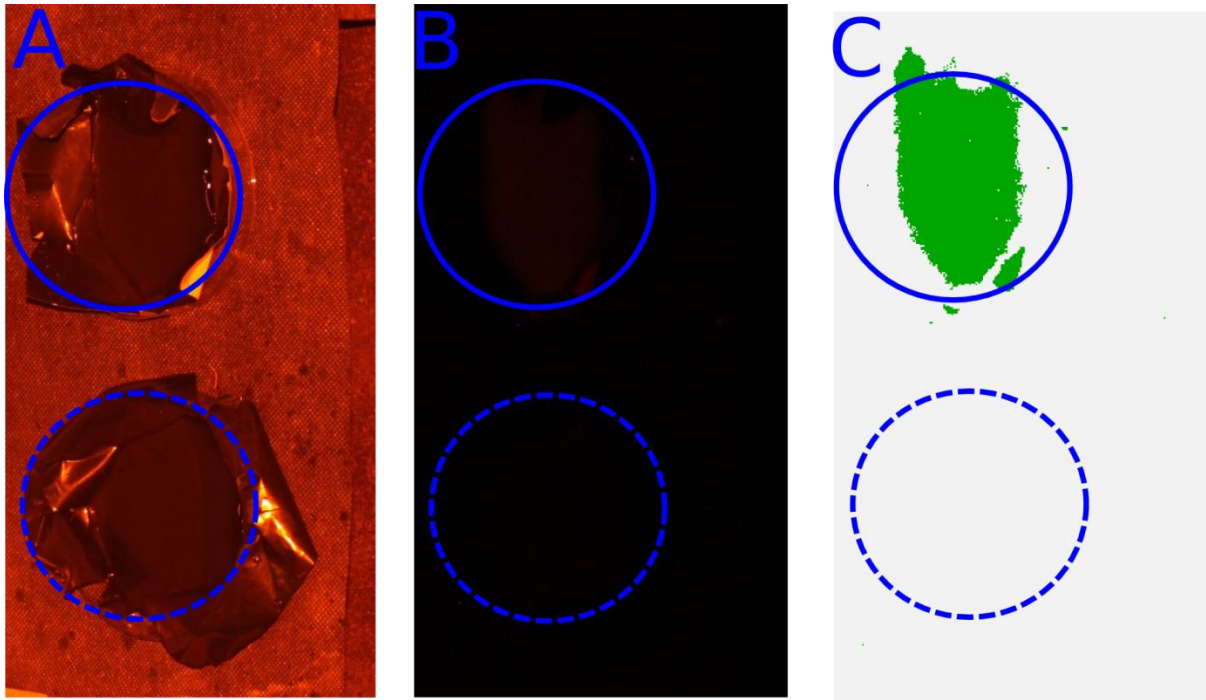
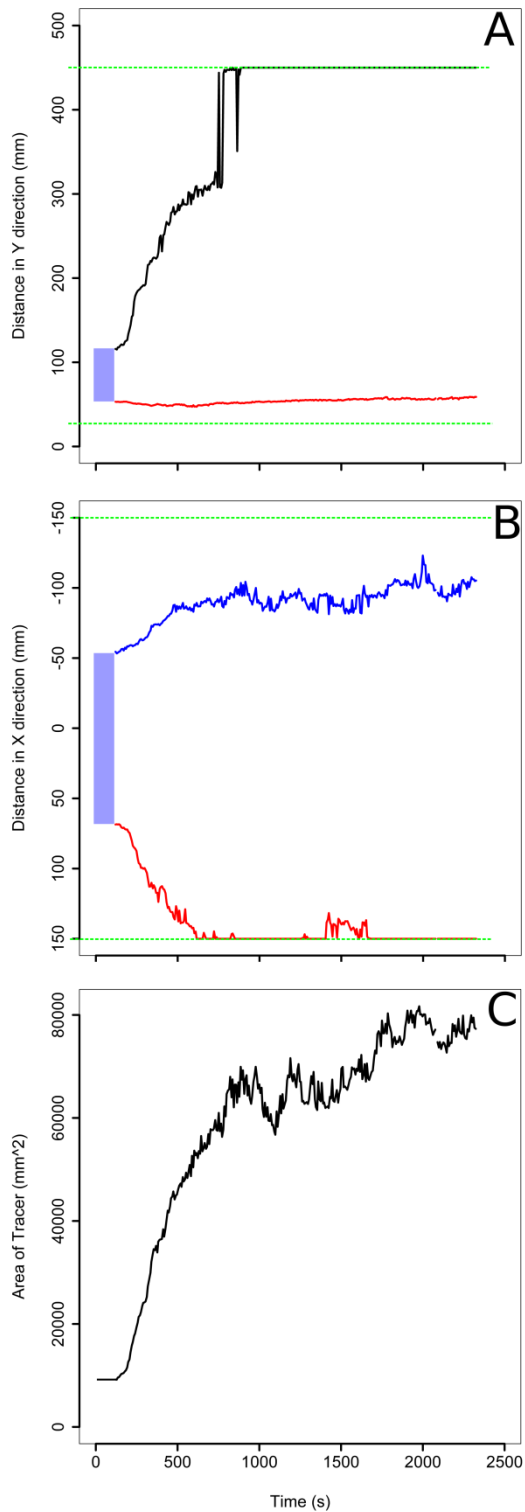


Figure 6. The movement of the tracer over time. The imageable area is bounded by the dashed green lines and the blue box represents the original location of the tracer. A shows the movement of the tracer in direction Y (the primary direction of water flow), B shows the lateral spread of tracer in direction X (orthogonal to the primary direction of water flow), and C shows the total area that the tracer occupies. All changes are shown against time.



1 A novel fluorescent tracer for real-time tracing of
2 clay transport over soil surfaces

3
4 *Robert A. Hardy¹, Jacqueline M. Pates¹, John N. Quinton^{1*}, Michael P. Coogan²*

5
6 ¹Lancaster Environment Center, Lancaster University, Bailrigg, LA1 4YQ

7 ²Chemistry Department, Lancaster University, Bailrigg, LA1 4YQ

8
9 * Corresponding author: j.quinton@lancaster.ac.uk

10
11 **KEYWORDS** Clay; tracing; soil erosion; diffuse pollution; fluorescence; tracer.

12

13

14 **ABSTRACT**

15 Clay is an important vector for the transport of pollutants in the environment, including
16 nutrients, pesticides and metals; therefore, the fate of many chemicals in soil systems is closely
17 linked to that of clay. Understanding the mechanisms responsible for clay transport has been
18 hampered by the lack of a suitable tracer. Producing a tracer that accurately mimics clay
19 transport is challenging, due to the small size of the particles and their unique physical
20 properties. Here we describe the design and synthesis of a tracer using natural clay particles as a
21 foundation, exploiting the natural ability of clay to sorb molecules to coat the clay with a thin
22 layer of fluorophore. Application of the tracer has been demonstrated through the collection of
23 real-time images of the tracer moving over the surface of a soil box during a rainfall event. These
24 images allow, for the first time, clay to be tracked spatially and temporally without need to
25 remove soil for analysis, thus resulting in minimal experimental artefacts. Custom written
26 software has been used to extract high resolution data describing tracer movement and extent
27 throughout the experiment.

28

29

30 **1. Introduction**

31 Clay is a key component of many of the world's soils. Its ability to sorb nutrients, such as
32 phosphorus (Sharpley et al., 1984; Sumner, 2000; Syers et al., 1971), potassium (Petrofanov,
33 2012), metals (Quinton and Catt, 2007) and organic pollutants (Homenauth and McBride, 1994;
34 Sumner, 2000), and its ease of transport in flowing water makes clay an important vector for
35 contaminant transport. Clay particles are moved by both overland flow (Quinton and Catt, 2007;
36 Quinton et al., 2001) and by subsurface flow (McCarthy and Zachara, 1989), which may connect
37 with rivers and lakes. Although studies have developed an empirical understanding of clay
38 movement (Quinton and Catt, 2007; Quinton et al., 2001) and there have been attempts to model
39 clay transport over and through soils (Jarvis et al., 1999; Jomaa et al., 2010), deriving spatial and
40 temporal distributions of clay movement in response to rainfall has proved elusive. In this paper
41 we describe a methodology, which, for the first time, allows the tracking of clay in time and
42 space across a soil surface.

43

44 *1.1 Tracing clay movement*

45 Tracing clay movement has proved very challenging (Armstrong et al., 2012). One aspect of this
46 challenge is the small size of the particles being traced. For larger particles (grains of sand size)
47 there has been success in mixing a dye with a binding agent and then applying this mixture to the
48 surface of the particles (Black et al., 2007). However, this technique has limitations for particles
49 that have a diameter of a few microns, as the coating significantly alters the size and density of
50 the particles. Therefore, for clay an alternative method of tracing is required.

51

52 This has led researchers to develop a range of techniques for tracing clay, including the use of
53 fluorescent microspheres (Burkhardt et al., 2008; Nielsen et al., 2011), rare earth oxides (REOs),
54 which, strictly speaking, are fine silt particles (Stevens and Quinton, 2008; Zhang et al., 2001),
55 and the labelling of clay particles with organic molecules (Selvam et al., 2008). The majority of
56 methods require sampling (via physical removal of material) of the soil after the experiment to
57 determine the tracer concentration (Mabit et al., 2013; Parsons and Foster, 2011). However, it is
58 desirable to understand how a process changes over time requiring the collection of dynamic
59 data. Sampling interferes with detachment and transport processes, limiting the use of existing
60 techniques for process studies. Therefore a method that does not require removal of material is
61 required if progress is to be made in understanding the dynamics of these processes. Additionally
62 there are significant density differences between tracers (such as microspheres and REOs) and
63 native clay particles, which are likely to affect their transport. Therefore a clay tracer with the
64 same physical and chemical properties as the native soil clay, and that can be manufactured
65 easily and analyzed using a non-invasive, non-destructive and in-situ analysis technique
66 operating at moderate to high temporal resolution, is desirable. Some progress has been made in
67 the nano-particle community with the creation of florescent nano-clays, however, no
68 environmental application of the material has been reported (Diaz et al., 2013).

69

70 *1.2 Fluorescence*

71 Fluorescence detection often allows for a high signal to noise ratio permitting single molecule
72 detection (Lakowicz, 2006). This sensitivity enables minimal fluorophore to be used in tracer
73 production, resulting in negligible modification of the coated particle. Traditionally, fluorescence
74 is measured on discrete samples using a fluorimeter, providing detailed spectral information.

75 Two previous studies have captured images of fluorescent tracers using film cameras. In the first,
76 silt-sized glass particles (44 to 2000 μm) labelled with uranium salts, which fluoresce under UV
77 light, were monitored on a 10 m slope inclined at 5.5% (Young and Holt, 1968). Later,
78 fluorescently-labelled pesticide granules (size unknown) were detected in soil, with each
79 photograph imaging 0.63 m^2 (Woods et al., 1999). This work assessed how soil tillage methods
80 affect incorporation of pesticide granules into soil; no effort was made to acquire images of the
81 pesticide moving.

82

83 *1.3 Fluorophore selection*

84 Four principle criteria were used to select the fluorophore. It should: bind strongly to clay;
85 fluoresce at a wavelength different to the auto-fluorescence of soil; be well characterized; and be
86 detectable using a CMOS (Complementary Metal Oxide Sensor) detector in a digital camera.
87 Successful binding relies on matching the fluorophore to the clay of interest; in general the
88 fluorophore should carry the opposite charge to the clay and be lipophilic. Soil auto-
89 fluorescence, due, in part, to the large quantity of organic aromatic acids that are present
90 (excitation maximum at 465 nm, emission maximum at 517 nm) (Milori et al., 2002; Rinnan and
91 Rinnan, 2007), can result in high background fluorescence and therefore interfere with detection
92 of the tracer. Therefore to reduce the impact of natural fluorescence a fluorophore that excites
93 between 520 and 600 nm was desired. Having a well characterized fluorophore allows more
94 rapid progress to be made as its chemical properties are already well described. Finally, we
95 wanted to use a CMOS detector array, commonly found in consumer grade cameras, as they
96 acquire images within the visible range (400-700 nm). A fluorophore that fluoresces in this range
97 was therefore required.

98

99 Rhodamine B was selected as the fluorophore, because: it binds to clay, e.g. Rhodamine B has
100 been shown to bond organically-modified montmorillonite (Diaz et al., 2013), and sodium
101 montmorillonite has been shown to be a successful remediation method for water contaminated
102 with Rhodamine B (Selvam et al., 2008); it typically has an excitation maximum around 570 nm
103 and emission maxima of around 590 nm (Beija et al., 2009), avoiding the most intense soil auto-
104 florescence; and it fluoresces within the range detectable by a CMOS detector. Many derivatives
105 have been synthesized, which could allow fine tuning of the clay tracer's fluorescent properties
106 (Beija et al., 2009), and it is commercially available and inexpensive.

107

108 **2. Materials and Methods**

109 Here we describe the materials and methods used to produce the clay-sized fluorescent tracer,
110 tests of its stability and its application to a laboratory scale erosion experiment.

111

112 The instruments used were an Agilent Technologies Cary Eclipse fluorescence spectrometer and
113 an Agilent Technologies Cary 60 UV/vis absorbance spectrophotometer. Disposable plastic
114 cuvettes were used throughout (Fisher Scientific). The water used was deionized water, unless
115 otherwise specified, and Rhodamine refers to Rhodamine B from Acros Organics (132311000).

116

117 *2.1 Tracer production*

118 The tracer was produced by sorbing Rhodamine onto the surface of clay particles. Twelve grams
119 montmorillonite (69904 ALDRICH) was ground to a fine powder, and sonicated for 30 minutes
120 in water. Rhodamine (0.2 g) was added and the volume made up to 1 L. The mixture was

121 sonicated for a further 45 minutes, stirred for 2 hours, then allowed to settle. The supernatant was
122 clear and colourless, and a vivid red-purple powder was visible at the bottom of the beaker.
123 Excess supernatant was decanted off and the powder collected using vacuum filtration through
124 two Whatman #5 filters. The filtrate was clear and colourless to the eye. The tracer was then
125 thoroughly rinsed using a 50:50 mixture of saturated NaCl and ethanol and then repeatedly with
126 water. The resulting tracer was dried at room temperature in a desiccator and protected from
127 light. If required, the tracer was gently disaggregated by hand before use.

128

129 *2.2 Tracer stability*

130 Stability tests were carried out to ensure the tracer would not degrade over the duration of the
131 trial (less than 24 hours). One gram of tracer (equivalent to 16.7 mg Rhodamine) was placed into
132 100 mL of solvent (either High Ionic Activity Solution (HIAS) or distilled water), and stirred to
133 mix. The HIAS was prepared by combining 25 g NaCl, 4.1 g Na₂SO₄, 0.7 g KCl, 11.2 g
134 MgCl₂·6H₂O and 2.3 g CaCl₂·6H₂O with deionised water to give a final volume of 1 L
135 (Sverdrup et al., 1942). The aim was to produce a simulated natural water of high ionic activity
136 with respect to the major elements. The concentrations used in this solution are extreme
137 compared to those normally found in terrestrial waters; if the tracer is stable under these
138 conditions, we assume that it will be stable in the vast majority of soil environments.

139

140 After a period of time (> 40 h), during which the tracer was allowed to settle, 3 mL of the
141 supernate was placed in a plastic cuvette to assess desorption of Rhodamine from the tracer,
142 using UV/vis absorbance spectrophotometry and fluorescence spectrometry. No attempt to

143 separate the tracer from the water was made, as any particles remaining in suspension were too
144 fine to remove by filtration.

145

146 To make calibration standards, first a stock solution was prepared by dissolving 18.2 mg
147 Rhodamine in 100 mL deionised water. Standards for UV/vis spectrophotometry and
148 fluorescence spectrometry were prepared by diluting the stock 1:250 for fluorescence
149 measurements and 1:125 for UV/vis measurements, using either HIAS or deionised water. Thus,
150 the UV/vis standards contained 0.144 mg Rhodamine per 100 mL, and the fluorescence
151 standards contained 0.072 mg Rhodamine per 100 mL. These are the concentrations that would
152 be achieved had 1% or 0.5% Rhodamine dissolved off the tracer during the stability experiments.

153

154 *2.3 Physical properties of tracer*

155 A Leica confocal microscope was used to record images of clay and tracer particles. Images
156 were taken using a 63x optical lens under oil. The size range of particles was measured using a
157 Malvern Mastersizer 2000.

158

159 *2.4 Acquiring fluorescent images*

160 Images were acquired using a Canon 500-D DSLR camera mounted on a tripod. (See
161 Supplementary Information (SI) 1: Camera setup, for further details of the camera settings and
162 filters). A ~75 mW, 532 nm (green) laser was used to illuminate the soil box, after passing
163 through a rotating diffuser (SI 2: Laser lighting setup, SI: Figure S1). Achieving uniform
164 illumination is critical to producing accurate images (Waters, 2009). Visual and photographic
165 assessment of the light showed an acceptable degree of uniformity (SI: Figure S2).

166

167 2.5 Soil box

168 Perspex soil boxes (350 mm by 500 mm), with drainage holes in the base, were filled with 4 cm
169 fine gravel, landscape fabric membrane, 3 cm sand and 4 cm soil (screened to 4 mm) to simulate
170 natural infiltration conditions following Armstrong *et al.*'s method (Armstrong et al., 2012). [The](#)
171 [soil was a clay loam soil of the Wick 1 association from Lancaster, Lancashire, United Kingdom.](#)

172 A 150 x 50 x 5 mm section of soil was removed, mixed with 4 g of tracer and then replaced
173 (Figure 1). To bring them to near saturation, the soil boxes were immersed in water, to a depth 1
174 cm above the soil-sand interface, for 22 hours. The box was then drained for one hour and
175 exposed to rainfall, while set at a slope of 4%.

176

177 2.6 Rainfall

178 A gravity-fed rainfall simulator was used to deliver rainfall with an intensity of 42 mm h⁻¹ using
179 reverse osmosis (RO) grade water (Armstrong et al., 2012).

180

181 2.7 Runoff testing

182 Runoff was collected from the run-off collector (Figure 1), with the container receiving the run-
183 off changed every 5 minutes. Runoff collected from between 30 and 45 minutes after rainfall has
184 commenced was bulked and vacuum filtered using two Whatman #5 filters to remove the
185 particulates.

186

187

188 **3. Results**

189 *3.1 Tracer stability*

190 In order for a tracer to be useful it must remain intact for the duration of the study. The most
191 likely route of tracer degradation is desorption of Rhodamine from the clay surface. To
192 investigate this possibility, UV/vis absorbance and fluorescence spectrometry were used to
193 characterize the loss of Rhodamine upon exposure to HIAS or distilled water (over 40 hours).

194

195 The supernate showed virtually no absorbance of light in the UV/vis range due to solution phase
196 Rhodamine, as demonstrated by the lack of a peak at ~ 560 nm (Figures 2a and b). Figure 2a
197 shows a raised baseline attributed to fine, colloidal-sized particulate matter (the tracer) remaining
198 in suspension scattering the light, a hypothesis supported by the lack of specific absorption
199 bands. The small peak at ~ 590 nm is assigned to Rhodamine as no other component absorbs in
200 that region. However the wavelength maximum does not match that of the Rhodamine standard,
201 which suggests that the Rhodamine responsible for this peak is modified compared to the
202 standard. An interaction between Rhodamine and montmorillonite, either through chemisorption
203 onto the surface, or simple protonation (the montmorillonite used is pH 3), could account for this
204 shifted wavelength. The absence of a raised baseline in HIAS (Figure 2b) suggests that there are
205 no tracer particles present; we propose that the high ionic strength of HIAS encourages
206 flocculation and hence precipitation out of the clay tracer (Elimelech et al., 1995).

207

208 Fluorescence measurements showed a peak with a maximum emission at 575 nm, attributed to
209 dissolved Rhodamine, in the HIAS solution (Figure 2d). In order to estimate the amount of
210 Rhodamine lost from the tracer during the experiment, linearity between the sample and standard

211 was assumed and the following equation used to estimate the amount of Rhodamine lost:
212 $(\text{standard concentration} / \text{fluorescence intensity of standard}) \times \text{fluorescence intensity of sample}$.
213 This relationship suggests that approximately 0.022 mg Rhodamine was lost from the tracer, i.e.
214 0.13% of the total amount used in the experiment. A broader and flatter peak is seen in the
215 deionized water sample (Figure 2c), indicative of minimal desorption from the tracer. The
216 greater desorption of Rhodamine in HIAS is probably due to the high ionic strength of the
217 solution, whereby the HIAS ions compete with the Rhodamine for binding sites on the clay
218 forcing the latter to desorb. However, HIAS has a much higher ionic strength than water soil
219 mixtures, where the tracer will be deployed; therefore it is reasonable to assume that desorption
220 will not readily occur during soil transport experiments.

221

222 *3.2 Physical properties of tracer*

223 Comparing the particle size distribution of the tracer and the clay from which the tracer was
224 made, it was found that 55% of the tracer had a size of less than 2 μm , compared to 51% of the
225 montmorillonite. Furthermore, the size distribution of the particles before and after treatment
226 with Rhodamine was consistent (SI 3: Tracer size). Confocal microscope images show that the
227 particles retain their irregular sizes and shapes (Figures 3a and b). The Rhodamine appears to be
228 uniformly distributed over the particle surface, without disturbing surface texture (Figure 3c).
229 The appearance of more rings around the clay in the phase contrast image of the tracer is
230 consistent with the hydration of the clay during synthesis of the tracer.

231

232 *3.3 Tracer movement images*

233 The images show, for the first time, clay movement over a soil surface in real time under
234 continuous simulated rainfall conditions (Figure 4 and SI 4: Images). The movement of tracer
235 across the whole soil box was recorded every 7 s from a distance of ~ 2 m. The sample area is
236 2431 x 1769 pixels (0.135 m²), which equates to approximately 31 pixels per mm². As no soil
237 was physically removed from the box during the experiment, there was no external disturbance
238 to the system, resulting in fewer sampling artefacts. By increasing the light input (by increasing
239 the camera aperture and moving the light source closer to the target) and sensitivity of the CMOS
240 detector (by increasing the ISO setting), the soil box was imaged on the sub-second time scale
241 (every 0.8 s), although increased noise was present (SI 5: Rapid imaging).

242

243 *3.4 Image processing*

244 Although it is possible to view the images without post-processing, much can be gained from
245 doing so. Using [R] (Hijmans, 2014; Polzehl and Tabelow, 2007; R Development Core Team,
246 2013; Urbanek, 2013), the images were converted to false colour with noise suppressed (Figure
247 4). Further details of the image processing methods can be found in SI 6: Image processing.
248 These images were easier to analyze visually, as they show presence of tracer in green and the
249 absence in white. The file size of the images is approximately 100 times smaller than the original
250 images. Images of this nature were then compressed (Cinepak codec by Radius, quality 100) into
251 a time-lapse video using VirtualDub (version 1.10.4) allowing the whole event to be reviewed in
252 less than a minute.

253

254 The intensity of fluorescence from the tracer, in the solid state, is independent of the
255 concentration of tracer. This type of behavior is symptomatic of self-quenching, which involves
256 the rapid exchange of energy between molecules and de-excitation via non-radiative processes,
257 typically relaxation to the ground state through vibrational levels. Due to the close spatial
258 proximity of the Rhodamine molecules to one another when bound to clay and the small Stokes
259 shift (and therefore overlap of excitation and emission bands), this type of behavior is neither
260 unusual nor unexpected (Lakowicz, 2006). As the amount of light emitted from the tracer is not a
261 function of the tracer concentration, the intensity of light cannot be used to quantify the amount
262 of tracer at a given point. Nonetheless, the true-colour images shown (Figures 4a-c) have some
263 qualitative properties, as areas that are much more intensely coloured are likely to contain more
264 tracer than those that are less intensely coloured.

265

266 We have confidence that interference due to autofluorescence was not a problem as we have
267 used constant illumination and the initial images (Figures 4a and 4d) show intense colour where
268 the tracer was applied and virtually no colour anywhere else.

269

270 *3.5 Runoff testing*

271 In order for the tracer to be useful it must remain intact throughout the experiment, which can be
272 evaluated by recovering the tracer afterwards. Particulate material recovered from the runoff,
273 was dried and photographed on a black (non-fluorescent) background (Figure S4). The colour
274 and intensity seen in Figure S4 are very similar to the colour and intensity seen in Figure 4,
275 suggesting that the tracer has remained intact throughout the experiment.

276

277 The filtrate was a reddish brown to the eye, which were attributed to fine particles, given that
278 they are illuminated when a ~ 1 mW (532 nm) laser beam is passed through the suspension (an
279 effect not seen in particle-free solutions). The filtrate was centrifuged at 15000 rpm for 99
280 minutes, the supernatant decanted and then imaged on a non-fluorescent background, using
281 standard image acquisition and processing parameters. No fluorescence was seen (Figure 5), in
282 contrast to a solution containing 2 µg/L Rhodamine, which could be readily detected. We are
283 therefore confident that the images in Figures 4 a, b, c are images of the Rhodamine-labeled clay
284 rather than Rhodamine in solution.

285

286 *3.6 Demonstration of application*

287 In order to demonstrate how high temporal and spatial resolution data can be used in the study of
288 soil erosion processes, the tracer front was mapped against time (Figure 6a). The data were
289 extracted from 312 images using a custom written function in [R] (SI 10: Tracking tracer
290 spread). The effect of rain-splash was analyzed by looking at how the tracer front moved up and
291 down the box (Figure 6a), which demonstrates the dynamic nature of both the upper and lower
292 tracer fronts. As expected the movement down the box is more rapid than that up the box. The
293 lower tracer front moves rapidly to begin with, slows and then moves rapidly again. We attribute
294 this behavior to changes in soil microtopography akin to a dam bursting, allowing overland flow
295 to connect with the bottom of the box and rapidly deliver the tracer. The spike at approximately
296 1000 s is attributed to an artefact in the data. Lateral spreading of the tracer was also noticed in
297 the images so a plot correlating the width of the tracer band to time was also produced (Figure
298 6b), as well as the changing tracer area over time (Figure 6c). The development of the tracer
299 area can viewed dynamically in the online version of the papers (video1).

300

301 4. Discussion

302 We have developed a tracing and imaging method that, for the first time, allows clay movement
303 to be traced, with mm precision in two dimensions with a time-step of approximately 1 s, under
304 simulated rainfall conditions without the need to stop the experiment to take samples. This is a
305 major advance over previously reported techniques. Previous work has focused on the use of
306 exotic particles and elemental tagging in soil tracing; examples include fluorescent microspheres
307 (Pryce, 2011), ceramic prills (Duke et al., 2000; Plante et al., 1999), plastic magnetic beads
308 (Ventura et al., 2001) and REOs (Deasy and Quinton, 2010). These methods have been criticized
309 as the tracers have different physical properties, such as size, shape and density, to the target soil
310 (Zhang et al., 2003). By using natural particles as the basis for this tracer we believe that we have
311 minimised or avoided many of these problems; physically, the tracer retains the same size and
312 density characteristics as the native clay and aggregates in the same way as the untreated clay.

313

314 The second advantage over existing methods is to ability to capture spatial information, without
315 the need to destructively sample the experiment, and temporal information throughout the
316 experiment, allowing highly dynamic changes in tracer distribution to be captured. ~~With~~
317 ~~the~~Other than work utilizing magnetic susceptibility e.g. exception of Armstrong et al. (e.g.
318 Armstrong et al., 2012), ~~who used magnetic susceptibility to non-destructively determine the~~
319 ~~position of a magnetic tracer at the end of an experiment,~~ experimenters have largely relied on
320 destructive sampling at the end of an experiment in order to understand surface processes.

321 Destructive sampling has limited spatial resolution, because of the size of samples required

322 (typically $> 2 \text{ cm}^2$), is laborious, and for many tracers requires subsequent analysis. The temporal

323 and spatial resolution of our tracer will allow us to gain insights into the controls on colloidal
324 detachment and transport, and have the potential to enable the spatial testing of distributed
325 models of size-selective erosion processes (Heng et al., 2011).

326
327 The system we have described is limited in scale to a 0.5 m x 0.4 m soil box, constrained by the
328 field of view of the camera as well as the area that can be illuminated with the laser. Larger fields
329 of view could be used to expand the area that can be imaged; however this would reduce the
330 resolution of the system. Working on larger study areas will require a brighter laser for
331 illumination and either multiple cameras to capture multiple images, which could be stitched
332 together in post-processing, or a super-camera with a large frame area and high density of pixels,
333 for example the qG (Aqueti Inc.), which is 250 megapixel camera with a 50 by 24 degree field of
334 view.

335
336 This new tracing methodology will open up new opportunities to understand clay transport and
337 associated pollutants and nutrients, helping us to develop a better understanding of these
338 dynamic processes. There is potential to develop the system further to provide a tracer and
339 detection method for field-based deployment and the quantification of tracer concentrations,
340 opening up new possibilities for understanding the fate and behavior of sediment and
341 contaminants in the environment.

342
343 **Supporting Information.** Diagrams relating to equipment design, camera and lighting
344 conditions, computer code, runoff testing and demonstration of application can be found in the
345 Supporting Information.

346

347 **Acknowledgments**

348 R.H. is funded by a joint U.K. Natural Environment Research Council – Analytical Chemistry
349 Trust Fund studentship (NE/J017795/1). Thanks to Mike James for his support with image
350 processing and Debbie Hurst for microscope images.

351

352 **References**

- 353 Armstrong, A., Quinton, J.N. and Maher, B.A., 2012. Thermal enhancement of natural
354 magnetism as a tool for tracing eroded soil. *Earth Surf. Proc. Land.* 37, 1567-1572.
- 355 Beija, M., Afonso, C.A.M. and Martinho, J.M.G., 2009. Synthesis and applications of
356 Rhodamine derivatives as fluorescent probes. *Chemical Soc. Rev.* 38, 2410-2433.
- 357 Black, K.S., Athey, S., Wilson, P. and Evans, D. (2007) *Coastal and Shelf Sediment Transport.*
358 Balson, P.S. and Collins, M.B. (eds), pp. 73-91, Geological Society, Special Publications,
359 London.
- 360 Burkhardt, M., Kasteel, R., Vanderborght, J. and Vereecken, H., 2008. Field study on colloid
361 transport using fluorescent microspheres. *Eur. J. Soil Sci.* 59, 82-93.
- 362 Deasy, C. and Quinton, J.N., 2010. Use of rare earth oxides as tracers to identify sediment source
363 areas for agricultural hillslopes. *Solid Earth* 1, 111-118.
- 364 Diaz, C.A., Xia, Y., Rubino, M., Auras, R., Jayaraman, K. and Hotchkiss, J., 2013. Fluorescent
365 labeling and tracking of nanoclay. 5, 164-168.
- 366 Duke, M.J.M., Plante, A.F. and McGill, W.B., 2000. Application of INAA in the characterisation
367 and quantification of Dy-labeled ceramic spheres and their use as inert tracers in soil
368 studies. *J. Radioanal. Nucl. Ch.* 244, 165-171.
- 369 Elimelech, M., Gregory, J., Jia, X. and Williams, J.A., 1995. *Particle Deposition and*
370 *Aggregation : Measurement, Modelling and Simulation*, Butterworth-Heinemann,
371 Oxford, England.
- 372 Heng, B.C.P., Sander, G.C., Armstrong, A., Quinton, J.N., Chandler, J.H. and Scott, C.F., 2011.
373 Modeling the dynamics of soil erosion and size-selective sediment transport over
374 nonuniform topography in flume-scale experiments. *Water Resources Res.* 47, W02513.
- 375 Hijmans, R.J. (2014) raster: raster: Geographic data analysis and modeling.
- 376 Homenauth, O.P. and McBride, M.B., 1994. Adsorption of aniline on layer silicate clays and an
377 organic soil. *Soil Sci. Soc. Am. J.* 58, 347-354.
- 378 Jarvis, N.J., Villholth, K.G. and Ulen, B., 1999. Modelling particle mobilization and leaching in
379 macroporous soil. *Eur. J. Soil Sci.* 50, 621-632.
- 380 Jomaa, S., Barry, D.A., Brovelli, A., Sander, G.C., Parlange, J.Y., Heng, B.C.P. and Tromp-van
381 Meerveld, H.J., 2010. Effect of raindrop splash and transversal width on soil erosion:
382 Laboratory flume experiments and analysis with the Hairsine-Rose model. *J. Hydrol.*
383 395, 117-132.
- 384 Lakowicz, J.R., 2006. *Principles of Fluorescence Spectroscopy*, Springer, New York.

385 Mabit, L., Meusburger, K., Fulajtar, E. and Alewell, C., 2013. The usefulness of ¹³⁷Cs as a tracer
386 for soil erosion assessment: A critical reply to Parsons and Foster (2011). *Earth-Sci. Rev.*
387 127, 300-307.

388 McCarthy, J.F. and Zachara, J.M., 1989. Subsurface transport of contaminants. Mobile colloids
389 in the subsurface environment may alter the transport of contaminants. *Environ. Sci.*
390 *Technol.* 23, 496-502.

391 Milori, D., Martin-Neto, L., Bayer, C., Mielniczuk, J. and Bagnato, V.S., 2002. Humification
392 degree of soil humic acids determined by fluorescence spectroscopy. *Soil Sci.* 167, 739-
393 749.

394 Nielsen, M.H., Styczen, M., Ernstsens, V., Petersen, C.T. and Hansen, S., 2011. Distribution of
395 bromide and microspheres along macropores in and between drain trenches. *Vadose Zone*
396 *J.* 10, 345-353.

397 Parsons, A.J. and Foster, I.D.L., 2011. What can we learn about soil erosion from the use of Cs-
398 137? *Earth-Sci. Rev.* 108, 101-113.

399 Petrofanov, V.L., 2012. Role of the soil particle-size fractions in the sorption and desorption of
400 potassium. *Eurasian Soil Sci.* 45, 598-611.

401 Plante, A.F., Duke, M.J.M. and McGill, W.B., 1999. A tracer sphere detectable by neutron
402 activation for soil aggregation and translocation studies. *Soil Sci. Soc. Am. J.* 63, 1284-
403 1290.

404 Polzehl, J. and Tabelow, K., 2007. Adaptive smoothing of digital images: the R package
405 *adimpro*. *J. Statistical Software.*

406 Pryce, O. (2011) Development of environmental tracers for sediments and phosphorus. PhD
407 thesis, Lancaster University.

408 Quinton, J.N. and Catt, J.A., 2007. Enrichment of heavy metals in sediment resulting from soil
409 erosion on agricultural fields. *Environ. Sci. Technol.* 41, 3495-3500.

410 Quinton, J.N., Catt, J.A. and Hess, T.M., 2001. The selective removal of phosphorus from soil: Is
411 event size important? *J. Environ. Qual.* 30, 538-545.

412 R Development Core Team (2013) *R: A Language and Environment for Statistical Computing.*

413 Rinnan, R. and Rinnan, Å., 2007. Application of near infrared reflectance (NIR) and
414 fluorescence spectroscopy to analysis of microbiological and chemical properties of
415 Arctic soil. *Soil Biol. Biochem.* 39, 1664-1673.

416 Selvam, P.P., Preethi, S., Basakaralingam, P., N.Thinakaran, Sivasamy, A. and Sivanesan, S.,
417 2008. Removal of rhodamine B from aqueous solution by adsorption onto sodium
418 montmorillonite. *J. Hazard. Mater.* 155, 39-44.

419 Sharpley, A.N., Smith, S.J., Stewart, B.A. and Mathers, A.C., 1984. Forms of phosphorus in soil
420 receiving cattle feedlot waste. *J. Environ. Qual.* 13, 211-215.

421 Stevens, C.J. and Quinton, J.N., 2008. Investigating source areas of eroded sediments transported
422 in concentrated overland flow using rare earth element tracers. *Catena* 74, 31-36.

423 Sumner, M.E., 2000. *Handbook of Soil Science*, CRC Press, Boca Raton, Fla.

424 Sverdrup, H.U., Johnson, M.W. and Fleming, R.H., 1942. *The Oceans, Their Physics,*
425 *Chemistry, and General Biology*, Prentice-Hall, inc., New York.

426 Syers, J.K., Evans, T.D., Williams, J.D. and Murdock, J.T., 1971. Phosphate sorption parameters
427 of representative soils from Rio Grande Do Sul, Brazil. *Soil Sci* 112, 267-275.

428 Urbanek, S. (2013) *tiff*: Read and write TIFF images.

429 Ventura, E., Nearing, M.A. and Norton, L.D., 2001. Developing a magnetic tracer to study soil
430 erosion. *Catena* 43, 277-291.

431 Waters, J.C., 2009. Accuracy and precision in quantitative fluorescence microscopy. *J. Cell Biol.*
432 185, 1135-1148.

433 Woods, S., Haydock, P.P.J., Evans, K., Robinson, R.C. and Dawkins, T.C.K., 1999. Use of
434 fluorescent tracer techniques and photography to assess the efficiency of tillage
435 incorporated granular nematicides into potato seed-beds. *Soil Tillage Res.* 51, 17-23.

436 Young, R.A. and Holt, R.F., 1968. Tracing soil movement with fluorescent glass particles. *Soil*
437 *Sci. Soc. Am. Pro.* 32, 600-602.

438 Zhang, X.C., Friedrich, J.M., Nearing, M.A. and Norton, L.D., 2001. Potential use of rare earth
439 oxides as tracers for soil erosion and aggregation studies. *Soil Sci. Soc. Am. J.* 65, 1508-
440 1515.

441 Zhang, X.C., Nearing, M.A., Polyakov, V.O. and Friedrich, J.M., 2003. Using rare-earth oxide
442 tracers for studying soil erosion dynamics. *Soil Sci Soc Am J* 67, 279-288.

443

Supplementary material for on-line publication only

[Click here to download Supplementary material for on-line publication only: Supporting information catena 1 sept 15.docx](#)

Video

[Click here to download Video: clay 0.08 real.avi](#)

1 A novel fluorescent tracer for real-time tracing of
2 clay transport over soil surfaces

3
4 *Robert A. Hardy¹, Jacqueline M. Pates¹, John N. Quinton^{1*}, Michael P. Coogan²*

5
6 ¹Lancaster Environment Center, Lancaster University, Bailrigg, LA1 4YQ

7 ²Chemistry Department, Lancaster University, Bailrigg, LA1 4YQ

8
9 * Corresponding author: j.quinton@lancaster.ac.uk

10
11 **KEYWORDS** Clay; tracing; soil erosion; diffuse pollution; fluorescence; tracer.

12

13

14 **ABSTRACT**

15 Clay is an important vector for the transport of pollutants in the environment, including
16 nutrients, pesticides and metals; therefore, the fate of many chemicals in soil systems is closely
17 linked to that of clay. Understanding the mechanisms responsible for clay transport has been
18 hampered by the lack of a suitable tracer. Producing a tracer that accurately mimics clay
19 transport is challenging, due to the small size of the particles and their unique physical
20 properties. Here we describe the design and synthesis of a tracer using natural clay particles as a
21 foundation, exploiting the natural ability of clay to sorb molecules to coat the clay with a thin
22 layer of fluorophore. Application of the tracer has been demonstrated through the collection of
23 real-time images of the tracer moving over the surface of a soil box during a rainfall event. These
24 images allow, for the first time, clay to be tracked spatially and temporally without need to
25 remove soil for analysis, thus resulting in minimal experimental artefacts. Custom written
26 software has been used to extract high resolution data describing tracer movement and extent
27 throughout the experiment.

28

29

30 **1. Introduction**

31 Clay is a key component of many of the world's soils. Its ability to sorb nutrients, such as
32 phosphorus (Sharpley et al., 1984; Sumner, 2000; Syers et al., 1971), potassium (Petrofanov,
33 2012), metals (Quinton and Catt, 2007) and organic pollutants (Homenauth and McBride, 1994;
34 Sumner, 2000), and its ease of transport in flowing water makes clay an important vector for
35 contaminant transport. Clay particles are moved by both overland flow (Quinton and Catt, 2007;
36 Quinton et al., 2001) and by subsurface flow (McCarthy and Zachara, 1989), which may connect
37 with rivers and lakes. Although studies have developed an empirical understanding of clay
38 movement (Quinton and Catt, 2007; Quinton et al., 2001) and there have been attempts to model
39 clay transport over and through soils (Jarvis et al., 1999; Jomaa et al., 2010), deriving spatial and
40 temporal distributions of clay movement in response to rainfall has proved elusive. In this paper
41 we describe a methodology, which, for the first time, allows the tracking of clay in time and
42 space across a soil surface.

43

44 *1.1 Tracing clay movement*

45 Tracing clay movement has proved very challenging (Armstrong et al., 2012). One aspect of this
46 challenge is the small size of the particles being traced. For larger particles (grains of sand size)
47 there has been success in mixing a dye with a binding agent and then applying this mixture to the
48 surface of the particles (Black et al., 2007). However, this technique has limitations for particles
49 that have a diameter of a few microns, as the coating significantly alters the size and density of
50 the particles. Therefore, for clay an alternative method of tracing is required.

51

52 This has led researchers to develop a range of techniques for tracing clay, including the use of
53 fluorescent microspheres (Burkhardt et al., 2008; Nielsen et al., 2011), rare earth oxides (REOs),
54 which, strictly speaking, are fine silt particles (Stevens and Quinton, 2008; Zhang et al., 2001),
55 and the labelling of clay particles with organic molecules (Selvam et al., 2008). The majority of
56 methods require sampling (via physical removal of material) of the soil after the experiment to
57 determine the tracer concentration (Mabit et al., 2013; Parsons and Foster, 2011). However, it is
58 desirable to understand how a process changes over time requiring the collection of dynamic
59 data. Sampling interferes with detachment and transport processes, limiting the use of existing
60 techniques for process studies. Therefore a method that does not require removal of material is
61 required if progress is to be made in understanding the dynamics of these processes. Additionally
62 there are significant density differences between tracers (such as microspheres and REOs) and
63 native clay particles, which are likely to affect their transport. Therefore a clay tracer with the
64 same physical and chemical properties as the native soil clay, and that can be manufactured
65 easily and analyzed using a non-invasive, non-destructive and in-situ analysis technique
66 operating at moderate to high temporal resolution, is desirable. Some progress has been made in
67 the nano-particle community with the creation of florescent nano-clays, however, no
68 environmental application of the material has been reported (Diaz et al., 2013).

69

70 *1.2 Fluorescence*

71 Fluorescence detection often allows for a high signal to noise ratio permitting single molecule
72 detection (Lakowicz, 2006). This sensitivity enables minimal fluorophore to be used in tracer
73 production, resulting in negligible modification of the coated particle. Traditionally, fluorescence
74 is measured on discrete samples using a fluorimeter, providing detailed spectral information.

75 Two previous studies have captured images of fluorescent tracers using film cameras. In the first,
76 silt-sized glass particles (44 to 2000 μm) labelled with uranium salts, which fluoresce under UV
77 light, were monitored on a 10 m slope inclined at 5.5% (Young and Holt, 1968). Later,
78 fluorescently-labelled pesticide granules (size unknown) were detected in soil, with each
79 photograph imaging 0.63 m^2 (Woods et al., 1999). This work assessed how soil tillage methods
80 affect incorporation of pesticide granules into soil; no effort was made to acquire images of the
81 pesticide moving.

82

83 *1.3 Fluorophore selection*

84 Four principle criteria were used to select the fluorophore. It should: bind strongly to clay;
85 fluoresce at a wavelength different to the auto-fluorescence of soil; be well characterized; and be
86 detectable using a CMOS (Complementary Metal Oxide Sensor) detector in a digital camera.
87 Successful binding relies on matching the fluorophore to the clay of interest; in general the
88 fluorophore should carry the opposite charge to the clay and be lipophilic. Soil auto-
89 fluorescence, due, in part, to the large quantity of organic aromatic acids that are present
90 (excitation maximum at 465 nm, emission maximum at 517 nm) (Milori et al., 2002; Rinnan and
91 Rinnan, 2007), can result in high background fluorescence and therefore interfere with detection
92 of the tracer. Therefore to reduce the impact of natural fluorescence a fluorophore that excites
93 between 520 and 600 nm was desired. Having a well characterized fluorophore allows more
94 rapid progress to be made as its chemical properties are already well described. Finally, we
95 wanted to use a CMOS detector array, commonly found in consumer grade cameras, as they
96 acquire images within the visible range (400-700 nm). A fluorophore that fluoresces in this range
97 was therefore required.

98

99 Rhodamine B was selected as the fluorophore, because: it binds to clay, e.g. Rhodamine B has
100 been shown to bond organically-modified montmorillonite (Diaz et al., 2013), and sodium
101 montmorillonite has been shown to be a successful remediation method for water contaminated
102 with Rhodamine B (Selvam et al., 2008); it typically has an excitation maximum around 570 nm
103 and emission maxima of around 590 nm (Beija et al., 2009), avoiding the most intense soil auto-
104 florescence; and it fluoresces within the range detectable by a CMOS detector. Many derivatives
105 have been synthesized, which could allow fine tuning of the clay tracer's fluorescent properties
106 (Beija et al., 2009), and it is commercially available and inexpensive.

107

108 **2. Materials and Methods**

109 Here we describe the materials and methods used to produce the clay-sized fluorescent tracer,
110 tests of its stability and its application to a laboratory scale erosion experiment.

111

112 The instruments used were an Agilent Technologies Cary Eclipse fluorescence spectrometer and
113 an Agilent Technologies Cary 60 UV/vis absorbance spectrophotometer. Disposable plastic
114 cuvettes were used throughout (Fisher Scientific). The water used was deionized water, unless
115 otherwise specified, and Rhodamine refers to Rhodamine B from Acros Organics (132311000).

116

117 *2.1 Tracer production*

118 The tracer was produced by sorbing Rhodamine onto the surface of clay particles. Twelve grams
119 montmorillonite (69904 ALDRICH) was ground to a fine powder, and sonicated for 30 minutes
120 in water. Rhodamine (0.2 g) was added and the volume made up to 1 L. The mixture was

121 sonicated for a further 45 minutes, stirred for 2 hours, then allowed to settle. The supernatant was
122 clear and colourless, and a vivid red-purple powder was visible at the bottom of the beaker.
123 Excess supernatant was decanted off and the powder collected using vacuum filtration through
124 two Whatman #5 filters. The filtrate was clear and colourless to the eye. The tracer was then
125 thoroughly rinsed using a 50:50 mixture of saturated NaCl and ethanol and then repeatedly with
126 water. The resulting tracer was dried at room temperature in a desiccator and protected from
127 light. If required, the tracer was gently disaggregated by hand before use.

128

129 *2.2 Tracer stability*

130 Stability tests were carried out to ensure the tracer would not degrade over the duration of the
131 trial (less than 24 hours). One gram of tracer (equivalent to 16.7 mg Rhodamine) was placed into
132 100 mL of solvent (either High Ionic Activity Solution (HIAS) or distilled water), and stirred to
133 mix. The HIAS was prepared by combining 25 g NaCl, 4.1 g Na₂SO₄, 0.7 g KCl, 11.2 g
134 MgCl₂·6H₂O and 2.3 g CaCl₂·6H₂O with deionised water to give a final volume of 1 L
135 (Sverdrup et al., 1942). The aim was to produce a simulated natural water of high ionic activity
136 with respect to the major elements. The concentrations used in this solution are extreme
137 compared to those normally found in terrestrial waters; if the tracer is stable under these
138 conditions, we assume that it will be stable in the vast majority of soil environments.

139

140 After a period of time (> 40 h), during which the tracer was allowed to settle, 3 mL of the
141 supernate was placed in a plastic cuvette to assess desorption of Rhodamine from the tracer,
142 using UV/vis absorbance spectrophotometry and fluorescence spectrometry. No attempt to

143 separate the tracer from the water was made, as any particles remaining in suspension were too
144 fine to remove by filtration.

145

146 To make calibration standards, first a stock solution was prepared by dissolving 18.2 mg
147 Rhodamine in 100 mL deionised water. Standards for UV/vis spectrophotometry and
148 fluorescence spectrometry were prepared by diluting the stock 1:250 for fluorescence
149 measurements and 1:125 for UV/vis measurements, using either HIAS or deionised water. Thus,
150 the UV/vis standards contained 0.144 mg Rhodamine per 100 mL, and the fluorescence
151 standards contained 0.072 mg Rhodamine per 100 mL. These are the concentrations that would
152 be achieved had 1% or 0.5% Rhodamine dissolved off the tracer during the stability experiments.

153

154 *2.3 Physical properties of tracer*

155 A Leica confocal microscope was used to record images of clay and tracer particles. Images
156 were taken using a 63x optical lens under oil. The size range of particles was measured using a
157 Malvern Mastersizer 2000.

158

159 *2.4 Acquiring fluorescent images*

160 Images were acquired using a Canon 500-D DSLR camera mounted on a tripod. (See
161 Supplementary Information (SI) 1: Camera setup, for further details of the camera settings and
162 filters). A ~75 mW, 532 nm (green) laser was used to illuminate the soil box, after passing
163 through a rotating diffuser (SI 2: Laser lighting setup, SI: Figure S1). Achieving uniform
164 illumination is critical to producing accurate images (Waters, 2009). Visual and photographic
165 assessment of the light showed an acceptable degree of uniformity (SI: Figure S2).

166

167 *2.5 Soil box*

168 Perspex soil boxes (350 mm by 500 mm), with drainage holes in the base, were filled with 4 cm
169 fine gravel, landscape fabric membrane, 3 cm sand and 4 cm soil (screened to 4 mm) to simulate
170 natural infiltration conditions following Armstrong *et al.*'s method (Armstrong et al., 2012). The
171 soil was a clay loam soil of the Wick 1 association from Lancaster, Lancashire, United Kingdom.
172 A 150 x 50 x 5 mm section of soil was removed, mixed with 4 g of tracer and then replaced
173 (Figure 1). To bring them to near saturation, the soil boxes were immersed in water, to a depth 1
174 cm above the soil-sand interface, for 22 hours. The box was then drained for one hour and
175 exposed to rainfall, while set at a slope of 4%.

176

177 *2.6 Rainfall*

178 A gravity-fed rainfall simulator was used to deliver rainfall with an intensity of 42 mm h⁻¹ using
179 reverse osmosis (RO) grade water (Armstrong et al., 2012).

180

181 *2.7 Runoff testing*

182 Runoff was collected from the run-off collector (Figure 1), with the container receiving the run-
183 off changed every 5 minutes. Runoff collected from between 30 and 45 minutes after rainfall has
184 commenced was bulked and vacuum filtered using two Whatman #5 filters to remove the
185 particulates.

186

187

188 **3. Results**

189 *3.1 Tracer stability*

190 In order for a tracer to be useful it must remain intact for the duration of the study. The most
191 likely route of tracer degradation is desorption of Rhodamine from the clay surface. To
192 investigate this possibility, UV/vis absorbance and fluorescence spectrometry were used to
193 characterize the loss of Rhodamine upon exposure to HIAS or distilled water (over 40 hours).

194

195 The supernate showed virtually no absorbance of light in the UV/vis range due to solution phase
196 Rhodamine, as demonstrated by the lack of a peak at ~ 560 nm (Figures 2a and b). Figure 2a
197 shows a raised baseline attributed to fine, colloidal-sized particulate matter (the tracer) remaining
198 in suspension scattering the light, a hypothesis supported by the lack of specific absorption
199 bands. The small peak at ~ 590 nm is assigned to Rhodamine as no other component absorbs in
200 that region. However the wavelength maximum does not match that of the Rhodamine standard,
201 which suggests that the Rhodamine responsible for this peak is modified compared to the
202 standard. An interaction between Rhodamine and montmorillonite, either through chemisorption
203 onto the surface, or simple protonation (the montmorillonite used is pH 3), could account for this
204 shifted wavelength. The absence of a raised baseline in HIAS (Figure 2b) suggests that there are
205 no tracer particles present; we propose that the high ionic strength of HIAS encourages
206 flocculation and hence precipitation out of the clay tracer (Elimelech et al., 1995).

207

208 Fluorescence measurements showed a peak with a maximum emission at 575 nm, attributed to
209 dissolved Rhodamine, in the HIAS solution (Figure 2d). In order to estimate the amount of
210 Rhodamine lost from the tracer during the experiment, linearity between the sample and standard

211 was assumed and the following equation used to estimate the amount of Rhodamine lost:
212 $(\text{standard concentration} / \text{fluorescence intensity of standard}) \times \text{fluorescence intensity of sample}$.
213 This relationship suggests that approximately 0.022 mg Rhodamine was lost from the tracer, i.e.
214 0.13% of the total amount used in the experiment. A broader and flatter peak is seen in the
215 deionized water sample (Figure 2c), indicative of minimal desorption from the tracer. The
216 greater desorption of Rhodamine in HIAS is probably due to the high ionic strength of the
217 solution, whereby the HIAS ions compete with the Rhodamine for binding sites on the clay
218 forcing the latter to desorb. However, HIAS has a much higher ionic strength than water soil
219 mixtures, where the tracer will be deployed; therefore it is reasonable to assume that desorption
220 will not readily occur during soil transport experiments.

221

222 *3.2 Physical properties of tracer*

223 Comparing the particle size distribution of the tracer and the clay from which the tracer was
224 made, it was found that 55% of the tracer had a size of less than 2 μm , compared to 51% of the
225 montmorillonite. Furthermore, the size distribution of the particles before and after treatment
226 with Rhodamine was consistent (SI 3: Tracer size). Confocal microscope images show that the
227 particles retain their irregular sizes and shapes (Figures 3a and b). The Rhodamine appears to be
228 uniformly distributed over the particle surface, without disturbing surface texture (Figure 3c).
229 The appearance of more rings around the clay in the phase contrast image of the tracer is
230 consistent with the hydration of the clay during synthesis of the tracer.

231

232 *3.3 Tracer movement images*

233 The images show, for the first time, clay movement over a soil surface in real time under
234 continuous simulated rainfall conditions (Figure 4 and SI 4: Images). The movement of tracer
235 across the whole soil box was recorded every 7 s from a distance of ~ 2 m. The sample area is
236 2431 x 1769 pixels (0.135 m²), which equates to approximately 31 pixels per mm². As no soil
237 was physically removed from the box during the experiment, there was no external disturbance
238 to the system, resulting in fewer sampling artefacts. By increasing the light input (by increasing
239 the camera aperture and moving the light source closer to the target) and sensitivity of the CMOS
240 detector (by increasing the ISO setting), the soil box was imaged on the sub-second time scale
241 (every 0.8 s), although increased noise was present (SI 5: Rapid imaging).

242

243 *3.4 Image processing*

244 Although it is possible to view the images without post-processing, much can be gained from
245 doing so. Using [R] (Hijmans, 2014; Polzehl and Tabelow, 2007; R Development Core Team,
246 2013; Urbanek, 2013), the images were converted to false colour with noise suppressed (Figure
247 4). Further details of the image processing methods can be found in SI 6: Image processing.
248 These images were easier to analyze visually, as they show presence of tracer in green and the
249 absence in white. The file size of the images is approximately 100 times smaller than the original
250 images. Images of this nature were then compressed (Cinepak codec by Radius, quality 100) into
251 a time-lapse video using VirtualDub (version 1.10.4) allowing the whole event to be reviewed in
252 less than a minute.

253

254 The intensity of fluorescence from the tracer, in the solid state, is independent of the
255 concentration of tracer. This type of behavior is symptomatic of self-quenching, which involves
256 the rapid exchange of energy between molecules and de-excitation via non-radiative processes,
257 typically relaxation to the ground state through vibrational levels. Due to the close spatial
258 proximity of the Rhodamine molecules to one another when bound to clay and the small Stokes
259 shift (and therefore overlap of excitation and emission bands), this type of behavior is neither
260 unusual nor unexpected (Lakowicz, 2006). As the amount of light emitted from the tracer is not a
261 function of the tracer concentration, the intensity of light cannot be used to quantify the amount
262 of tracer at a given point. Nonetheless, the true-colour images shown (Figures 4a-c) have some
263 qualitative properties, as areas that are much more intensely coloured are likely to contain more
264 tracer than those that are less intensely coloured.

265

266 We have confidence that interference due to autofluorescence was not a problem as we have
267 used constant illumination and the initial images (Figures 4a and 4d) show intense colour where
268 the tracer was applied and virtually no colour anywhere else.

269

270 *3.5 Runoff testing*

271 In order for the tracer to be useful it must remain intact throughout the experiment, which can be
272 evaluated by recovering the tracer afterwards. Particulate material recovered from the runoff,
273 was dried and photographed on a black (non-fluorescent) background (Figure S4). The colour
274 and intensity seen in Figure S4 are very similar to the colour and intensity seen in Figure 4,
275 suggesting that the tracer has remained intact throughout the experiment.

276

277 The filtrate was a reddish brown to the eye, which were attributed to fine particles, given that
278 they are illuminated when a ~ 1 mW (532 nm) laser beam is passed through the suspension (an
279 effect not seen in particle-free solutions). The filtrate was centrifuged at 15000 rpm for 99
280 minutes, the supernatant decanted and then imaged on a non-fluorescent background, using
281 standard image acquisition and processing parameters. No fluorescence was seen (Figure 5), in
282 contrast to a solution containing 2 µg/L Rhodamine, which could be readily detected. We are
283 therefore confident that the images in Figures 4 a, b, c are images of the Rhodamine-labeled clay
284 rather than Rhodamine in solution.

285

286 *3.6 Demonstration of application*

287 In order to demonstrate how high temporal and spatial resolution data can be used in the study of
288 soil erosion processes, the tracer front was mapped against time (Figure 6a). The data were
289 extracted from 312 images using a custom written function in [R] (SI 10: Tracking tracer
290 spread). The effect of rain-splash was analyzed by looking at how the tracer front moved up and
291 down the box (Figure 6a), which demonstrates the dynamic nature of both the upper and lower
292 tracer fronts. As expected the movement down the box is more rapid than that up the box. The
293 lower tracer front moves rapidly to begin with, slows and then moves rapidly again. We attribute
294 this behavior to changes in soil microtopography akin to a dam bursting, allowing overland flow
295 to connect with the bottom of the box and rapidly deliver the tracer. The spike at approximately
296 1000 s is attributed to an artefact in the data. Lateral spreading of the tracer was also noticed in
297 the images so a plot correlating the width of the tracer band to time was also produced (Figure
298 6b), as well as the changing tracer area over time (Figure 6c). The development of the tracer
299 area can viewed dynamically in the online version of the papers (video1).

300

301 **4. Discussion**

302 We have developed a tracing and imaging method that, for the first time, allows clay movement
303 to be traced, with mm precision in two dimensions with a time-step of approximately 1 s, under
304 simulated rainfall conditions without the need to stop the experiment to take samples. This is a
305 major advance over previously reported techniques. Previous work has focused on the use of
306 exotic particles and elemental tagging in soil tracing; examples include fluorescent microspheres
307 (Pryce, 2011), ceramic prills (Duke et al., 2000; Plante et al., 1999), plastic magnetic beads
308 (Ventura et al., 2001) and REOs (Deasy and Quinton, 2010). These methods have been criticized
309 as the tracers have different physical properties, such as size, shape and density, to the target soil
310 (Zhang et al., 2003). By using natural particles as the basis for this tracer we believe that we have
311 minimised or avoided many of these problems; physically, the tracer retains the same size and
312 density characteristics as the native clay and aggregates in the same way as the untreated clay.

313

314 The second advantage over existing methods is to ability to capture spatial information, without
315 the need to destructively sample the experiment, and temporal information throughout the
316 experiment, allowing highly dynamic changes in tracer distribution to be captured. Other than
317 work utilizing magnetic susceptibility (e.g. Armstrong et al., 2012), experimenters have largely
318 relied on destructive sampling at the end of an experiment in order to understand surface
319 processes. Destructive sampling has limited spatial resolution, because of the size of samples
320 required (typically $> 2 \text{ cm}^2$), is laborious, and for many tracers requires subsequent analysis. The
321 temporal and spatial resolution of our tracer will allow us to gain insights into the controls on

322 colloidal detachment and transport, and have the potential to enable the spatial testing of
323 distributed models of size-selective erosion processes (Heng et al., 2011).

324

325 The system we have described is limited in scale to a 0.5 m x 0.4 m soil box, constrained by the
326 field of view of the camera as well as the area that can be illuminated with the laser. Larger fields
327 of view could be used to expand the area that can be imaged; however this would reduce the
328 resolution of the system. Working on larger study areas will require a brighter laser for
329 illumination and either multiple cameras to capture multiple images, which could be stitched
330 together in post-processing, or a super-camera with a large frame area and high density of pixels,
331 for example the qG (Aqueti Inc.), which is 250 megapixel camera with a 50 by 24 degree field of
332 view.

333

334 This new tracing methodology will open up new opportunities to understand clay transport and
335 associated pollutants and nutrients, helping us to develop a better understanding of these
336 dynamic processes. There is potential to develop the system further to provide a tracer and
337 detection method for field-based deployment and the quantification of tracer concentrations,
338 opening up new possibilities for understanding the fate and behavior of sediment and
339 contaminants in the environment.

340

341 **Supporting Information.** Diagrams relating to equipment design, camera and lighting
342 conditions, computer code, runoff testing and demonstration of application can be found in the
343 Supporting Information.

344

345 **Acknowledgments**

346 R.H. is funded by a joint U.K. Natural Environment Research Council – Analytical Chemistry
347 Trust Fund studentship (NE/J017795/1). Thanks to Mike James for his support with image
348 processing and Debbie Hurst for microscope images.

349

350 **References**

- 351 Armstrong, A., Quinton, J.N. and Maher, B.A., 2012. Thermal enhancement of natural
352 magnetism as a tool for tracing eroded soil. *Earth Surf. Proc. Land.* 37, 1567-1572.
- 353 Beija, M., Afonso, C.A.M. and Martinho, J.M.G., 2009. Synthesis and applications of
354 Rhodamine derivatives as fluorescent probes. *Chemical Soc. Rev.* 38, 2410-2433.
- 355 Black, K.S., Athey, S., Wilson, P. and Evans, D. (2007) *Coastal and Shelf Sediment Transport.*
356 Balson, P.S. and Collins, M.B. (eds), pp. 73-91, Geological Society, Special Publications,
357 London.
- 358 Burkhardt, M., Kasteel, R., Vanderborght, J. and Vereecken, H., 2008. Field study on colloid
359 transport using fluorescent microspheres. *Eur. J. Soil Sci.* 59, 82-93.
- 360 Deasy, C. and Quinton, J.N., 2010. Use of rare earth oxides as tracers to identify sediment source
361 areas for agricultural hillslopes. *Solid Earth* 1, 111-118.
- 362 Diaz, C.A., Xia, Y., Rubino, M., Auras, R., Jayaraman, K. and Hotchkiss, J., 2013. Fluorescent
363 labeling and tracking of nanoclay. *5*, 164-168.
- 364 Duke, M.J.M., Plante, A.F. and McGill, W.B., 2000. Application of INAA in the characterisation
365 and quantification of Dy-labeled ceramic spheres and their use as inert tracers in soil
366 studies. *J. Radioanal. Nucl. Ch.* 244, 165-171.
- 367 Elimelech, M., Gregory, J., Jia, X. and Williams, J.A., 1995. *Particle Deposition and*
368 *Aggregation : Measurement, Modelling and Simulation*, Butterworth-Heinemann,
369 Oxford, England.
- 370 Heng, B.C.P., Sander, G.C., Armstrong, A., Quinton, J.N., Chandler, J.H. and Scott, C.F., 2011.
371 Modeling the dynamics of soil erosion and size-selective sediment transport over
372 nonuniform topography in flume-scale experiments. *Water Resources Res.* 47, W02513.
- 373 Hijmans, R.J. (2014) raster: raster: Geographic data analysis and modeling.
- 374 Homenauth, O.P. and McBride, M.B., 1994. Adsorption of aniline on layer silicate clays and an
375 organic soil. *Soil Sci. Soc. Am. J.* 58, 347-354.
- 376 Jarvis, N.J., Villholth, K.G. and Ulen, B., 1999. Modelling particle mobilization and leaching in
377 macroporous soil. *Eur. J. Soil Sci.* 50, 621-632.
- 378 Jomaa, S., Barry, D.A., Brovelli, A., Sander, G.C., Parlange, J.Y., Heng, B.C.P. and Tromp-van
379 Meerveld, H.J., 2010. Effect of raindrop splash and transversal width on soil erosion:
380 Laboratory flume experiments and analysis with the Hairsine-Rose model. *J. Hydrol.*
381 395, 117-132.
- 382 Lakowicz, J.R., 2006. *Principles of Fluorescence Spectroscopy*, Springer, New York.

383 Mabit, L., Meusburger, K., Fulajtar, E. and Alewell, C., 2013. The usefulness of ¹³⁷Cs as a tracer
384 for soil erosion assessment: A critical reply to Parsons and Foster (2011). *Earth-Sci. Rev.*
385 127, 300-307.

386 McCarthy, J.F. and Zachara, J.M., 1989. Subsurface transport of contaminants. Mobile colloids
387 in the subsurface environment may alter the transport of contaminants. *Environ. Sci.*
388 *Technol.* 23, 496-502.

389 Milori, D., Martin-Neto, L., Bayer, C., Mielniczuk, J. and Bagnato, V.S., 2002. Humification
390 degree of soil humic acids determined by fluorescence spectroscopy. *Soil Sci.* 167, 739-
391 749.

392 Nielsen, M.H., Styczen, M., Ernstsens, V., Petersen, C.T. and Hansen, S., 2011. Distribution of
393 bromide and microspheres along macropores in and between drain trenches. *Vadose Zone*
394 *J.* 10, 345-353.

395 Parsons, A.J. and Foster, I.D.L., 2011. What can we learn about soil erosion from the use of Cs-
396 137? *Earth-Sci. Rev.* 108, 101-113.

397 Petrofanov, V.L., 2012. Role of the soil particle-size fractions in the sorption and desorption of
398 potassium. *Eurasian Soil Sci.* 45, 598-611.

399 Plante, A.F., Duke, M.J.M. and McGill, W.B., 1999. A tracer sphere detectable by neutron
400 activation for soil aggregation and translocation studies. *Soil Sci. Soc. Am. J.* 63, 1284-
401 1290.

402 Polzehl, J. and Tabelow, K., 2007. Adaptive smoothing of digital images: the R package
403 *adimpro*. *J. Statistical Software*.

404 Pryce, O. (2011) Development of environmental tracers for sediments and phosphorus. PhD
405 thesis, Lancaster University.

406 Quinton, J.N. and Catt, J.A., 2007. Enrichment of heavy metals in sediment resulting from soil
407 erosion on agricultural fields. *Environ. Sci. Technol.* 41, 3495-3500.

408 Quinton, J.N., Catt, J.A. and Hess, T.M., 2001. The selective removal of phosphorus from soil: Is
409 event size important? *J. Environ. Qual.* 30, 538-545.

410 R Development Core Team (2013) *R: A Language and Environment for Statistical Computing*.

411 Rinnan, R. and Rinnan, Å., 2007. Application of near infrared reflectance (NIR) and
412 fluorescence spectroscopy to analysis of microbiological and chemical properties of
413 Arctic soil. *Soil Biol. Biochem.* 39, 1664-1673.

414 Selvam, P.P., Preethi, S., Basakaralingam, P., N.Thinakaran, Sivasamy, A. and Sivanesan, S.,
415 2008. Removal of rhodamine B from aqueous solution by adsorption onto sodium
416 montmorillonite. *J. Hazard. Mater.* 155, 39-44.

417 Sharpley, A.N., Smith, S.J., Stewart, B.A. and Mathers, A.C., 1984. Forms of phosphorus in soil
418 receiving cattle feedlot waste. *J. Environ. Qual.* 13, 211-215.

419 Stevens, C.J. and Quinton, J.N., 2008. Investigating source areas of eroded sediments transported
420 in concentrated overland flow using rare earth element tracers. *Catena* 74, 31-36.

421 Sumner, M.E., 2000. *Handbook of Soil Science*, CRC Press, Boca Raton, Fla.

422 Sverdrup, H.U., Johnson, M.W. and Fleming, R.H., 1942. *The Oceans, Their Physics,*
423 *Chemistry, and General Biology*, Prentice-Hall, inc., New York.

424 Syers, J.K., Evans, T.D., Williams, J.D. and Murdock, J.T., 1971. Phosphate sorption parameters
425 of representative soils from Rio Grande Do Sul, Brazil. *Soil Sci* 112, 267-275.

426 Urbanek, S. (2013) *tiff*: Read and write TIFF images.

427 Ventura, E., Nearing, M.A. and Norton, L.D., 2001. Developing a magnetic tracer to study soil
428 erosion. *Catena* 43, 277-291.

429 Waters, J.C., 2009. Accuracy and precision in quantitative fluorescence microscopy. *J. Cell Biol.*
430 185, 1135-1148.

431 Woods, S., Haydock, P.P.J., Evans, K., Robinson, R.C. and Dawkins, T.C.K., 1999. Use of
432 fluorescent tracer techniques and photography to assess the efficiency of tillage
433 incorporated granular nematicides into potato seed-beds. *Soil Tillage Res.* 51, 17-23.

434 Young, R.A. and Holt, R.F., 1968. Tracing soil movement with fluorescent glass particles. *Soil*
435 *Sci. Soc. Am. Pro.* 32, 600-602.

436 Zhang, X.C., Friedrich, J.M., Nearing, M.A. and Norton, L.D., 2001. Potential use of rare earth
437 oxides as tracers for soil erosion and aggregation studies. *Soil Sci. Soc. Am. J.* 65, 1508-
438 1515.

439 Zhang, X.C., Nearing, M.A., Polyakov, V.O. and Friedrich, J.M., 2003. Using rare-earth oxide
440 tracers for studying soil erosion dynamics. *Soil Sci Soc Am J* 67, 279-288.

441